STABILITY OF FIELD EMITTER ARRAYS TO OXYGEN EXPOSURES

Soumitra Kumar Godbole, BTech

Thesis Prepared for the Degree of

MASTER OF SCIENCE

UNIVERSITY OF NORTH TEXAS

December 2002

APPROVED:

Bruce E. Gnade, Major Professor and Committee Member
Robert M. Wallace, Minor Professor
Mohamed El Bouanani, Committee Member
Michael Fanelli, Committee Member
Nandika A. D'Souza, Coordinator of the Program in Materials Science
Bruce E. Gnade, Chair of the Materials Science Department
C. Neal Tate, Dean of the Robert B. Toulouse School of Graduate Studies

Godbole, Soumitra Kumar, Stability of Field Emitter Arrays to Oxygen Exposures. Master of Science (Materials Science), December 2002, 88 pp., 3 tables, 48 illustrations, references, 74 titles.

The purpose of these experiments was to determine the degradation mechanisms of molybdenum based field emitter arrays to oxygen exposures and to improve the overall reliability. In addition, we also evaluated the emission current stability of gold-coated field emitter arrays to oxygen exposures.

To ensure identical oxygen exposure and experimental measurement conditions, tips on half the area of the FEA were fully coated with gold and the other half were left uncoated. The emission current from the gold coated half was found to degrade much less than that from the uncoated half, in the presence of oxygen. Also, in the absence of oxygen, the emission current recovery for the gold-coated half was much quicker than that for the uncoated half.

ACKNOWLEDGMENTS

I have a number of persons to thank for helping me to achieve my goal in life. First of all, I would like to thank my advisor: Dr. Bruce Gnade, who apart from providing me the opportunity to be a part of his group, has been of invaluable help both in research and finding me new opportunities for the future.

Dr. Robert Wallace, who has also been my co-advisor for this work, has been of great help in my research. He showed me not only how to work with and setup equipment, but also to troubleshoot problems efficiently and systematically. His amazing approach of solving a problem by getting to the very root was of immense help in making theoretical concepts clear and correlating them with experimental data.

I would also like to thank Dr. Nasrazadani for all his help during the initial stages of this work. He has been jovial, encouraging and fun to work with. I am grateful to Dr. Edward Sosa, who in spite of his busy schedule, always helped us in our research and has been instrumental in setting up our Power Supply programmer.

I wish to thank Dr. Manuel Quevedo and Dr. Mohammed El Bouanani who have been of great help not only in my research as they carried out RBS for determining the gold thickness deposited on the FEAs, but also shared with me their expertise and helped in writing this thesis. I also wish to thank Dr. Swarna Addepalli, who was very helpful with obtaining the references listed.

I am thankful to Billy Raulston and Tommy Bennett for their excellent machine shop service, because of which we could perform our experiments. I am also grateful to Tom Schrimsher for all his help with troubleshooting and wizardry in electronics.

I wish to thank Kevin Chapla for all his help during the latter stages of this research. He made wonderful modifications to the already existing UHV chamber, one of which was introducing a load-lock. I also wish like to thank Prasanna Vemuri who has been extremely helpful during the later part of this work. It was because of her sincere effort that we were able to have the system running again after it was moved.

During the course of my internship at Zyvex, I would like to thank Dr. Christof Baur and Dr. Richard Stallcup for sharing with me, their amazing research skills. I am also grateful to Evan Carey for sharing with me, his wizardry in Labview and excellent programming skills, which was of great help in data acquisition.

I wish to thank my fellow Teaching Assistants in Astronomy - Gerardo Aquino, and Arne Schwettman for their help in rescheduling the labs so I could complete my thesis on time. I also wish to thank Jophy Augustine, Noel Nicholson, Nicola Scafetta, Filippo Giraldi and Mauro Bologna for their affection and friendship.

I thank the committee members - Dr. Mohammed El Bouanani and Dr. Michael Fanelli for their suggestions, which made this thesis clear and presentable. I would also like to thank Gaurang Pant, Dr. Prakaiketch Puchaipetch, Alberta Caswell and the Materials Science staff, for being very helpful during my graduate study at UNT. Lastly, I would like to thank my family for supporting my pursuit for graduate study in the US.

TABLE OF CONTENTS

Page

LIST OF TABLES

Table Page

LIST OF ILLUSTRATIONS

CHAPTER 1

INTRODUCTION

1.1. Introduction

Spindt-type Mo field emission micro cathode arrays (FEAs) are being pursued as high brightness electron sources in applications ranging from field emission displays to high-speed RF devices.[1,2] The driving force behind the current interest in field emission arrays is to develop high-resolution field emission flat panel displays.

The Spindt deposition process has enabled the production of Mo field emitter arrays made with micron sized field emitters.[3] The present problem with Mo field emitter tips is the degradation in emission current, mainly due to oxidation. For these reasons, various materials ranging from metals to semiconductors have been investigated. Field emission is sensitive to both changes in composition and structure of the emitting surface.[4, 5, 6]

1.2. Selection of Field Emitter materials

Currently, Mo field emitter arrays are used because of their good thermal, mechanical and electrical properties. Mo has a moderate work function of 4.6 eV, which is a very important parameter for selecting field emitter materials. Mo has a low resistivity and a high melting point, thus high currents can be sustained without tip failures.[7]

Mo is compatible with common microelectronic manufacturing processing, allowing field emission arrays made with Mo emitters to be readily produced using standard semiconductor process equipment. Furthermore, Mo can be easily deposited

using standard semi-conductor technology. Also, a high aspect ratio (the ratio of the base diameter to the tip height) can be achieved using Mo tips.

Unfortunately, Mo is known to oxidize readily in the presence of O_2 forming MoO_2 and MoO_3.[8,9,10] The oxidation of Mo tips is one of the main reasons for emission current instability in Mo FEAs. Therefore, in order to use Mo as a field emission material for commercial displays, its oxidation must be limited, if not prevented.

One possible way to limit oxidation is to coat the Mo tip with a thin film of a noble metal. The coating should be easy to deposit at moderately high temperatures, uniform, and stable. The deposited metal should also have a comparable or lower work function, as Mo. Au is such a metal that satisfies most of the above requirements, in spite of having a higher work function.

1.3. Oxidation of Field Emitter Tips

Field emission is the tunneling of electrons from the metal into vacuum under the influence of a very high electric field (see chapter 2). The emission current strongly depends on the work function of the surface, thus field emission arrays are extremely sensitive to contamination of the tips by O_2 present in the vacuum environment.[11,12] One of the effects of O_2 is tip oxidation. The oxide (MoO_2) has a higher work function, and this leads to a significant reduction in emission current.

One of the main reasons for degradation in emission current is the oxidation of the Mo emitter tips. The impact of these ions on the tips causes surface modifications leading to emission current instabilities and subsequent device failures.[13] Thus a fundamental understanding of the sensitivity of the field emission arrays to O_2 is required in determining the long-term emission current stability and the device reliability.

Similar vacuum problems have been encountered during the development of reliable thermionic cathodes for vacuum tube electronics. Extensive studies have been made on the effects of residual gases on electron emission characteristics of W and BaO type impregnated thermionic cathodes.[14] It has been clearly established that gases like H_2 and CH_4 enhance the emission current, while gases like O_2, H_2O and CO_2 which act as oxidizing agents on metals, cause serious poisoning of thermionic cathodes.[15,16,17]

Exposures to O_2 cause serious emission degradation for thermionic cathodes.[18] The vacuum issues are much more serious in the case of field emission arrays. The presence of high electric fields and high-density electron beams result in the dissociation and ionization of the residual gases. Also, the fact that FEAs operate at low temperature means high sticking coefficient for these residual gases.

The impact of these ions on the tips leads to tip shape and surface modifications resulting in serious emission degradation and emission current instabilities. Thus, reliable data on the lifetime of the devices in an O_2 environment is required in order to establish the vacuum requirements for the successful operation of devices based on FEAs.[18]

1.4. Surface Physics of Field Emission Microcathode Arrays

A discussion of the critical problems related to the long-term reliability and device stability issues is outlined. The challenges to the integration of FEA technologies into applications like high-resolution displays are discussed.

Brodie and Spindt[2] have presented a comprehensive review of the technology of vacuum microelectronic devices and Schwoebel and Brodie[13] have discussed some of the important issues and related surface science aspects of vacuum microelectronic devices.

The residual gas environment within the device during cathode operation can significantly impact the long-term current stability and the lifetime of these arrays.

A problem of scientific and technological interest is the effect of gaseous exposures and the resulting emission changes from the FEAs. The interaction of residual gases with the field emitter arrays modifies the work function of the tip surfaces and emission current changes according to the Fowler-Nordheim tunneling equations.[19] Thus, a careful study of the effect of various gases on the emission characteristics and the resulting change in work function is needed.

High field-induced chemical reactions also play an important role in determining the surface chemistry and physics of these devices during their operation.[20] In a typical Spindt-type cathode array, the anode to tip spacing is about 0.5? m. For gate voltages of 50 to 100 V, electric fields as high as 10^8 V /m can be achieved near the tips. With such high fields, field dissociation of gases can occur near the emitter surface.[21]

The resulting ions and free radicals can further modify the geometry of tip surfaces and change the work function and thus the emission. Ion impact on the field emitter tips is thought to be responsible for current instabilities and subsequent device failures in FEAs.[13,22]

The interaction of O_2 with Mo has been extensively studied to understand the oxidation and formation of Mo oxide.[9,23,24,25,26] The interaction of O_2 with Mo in the presence of high electric fields was studied by Okuyama using field emission spectroscopy.[27] He found that the reaction results in the formation of Mo oxide surface layers. This was further investigated by Chalamala *et. al,* who did similar experiments using FEAs and reported the detrimental effects of O_2.[18]

1.5. Scope of the Present Work

The purpose of this work is to study and compare the interaction of Au coated and uncoated Mo field emitter arrays with O_2. In our experiments, we tested several FEAs, some coated with Au on one half and the other half uncoated. In this way we can make our measurements with identical conditions on both the Au coated half and the uncoated half simultaneously. The experimental work permitted us to measure the emission characteristics of the FEAs as a function of the gas exposure dose.

The total exposure dose was calculated by simply multiplying the O_2 partial pressure by the exposure time in seconds and then dividing by 1.0×10^{-6} torr to get the exposure dose in Langmuirs (L). One Langmuir is defined as the dose for an exposure of 1? torr O_2 for one second. Assuming the O_2 pressure to be constant at 1.0×10^{-6} torr, gives us an inaccurate value for the exposure dose during the initial part of the experiment, as there are high O_2 pressure fluctuations. Also, the degradation in emission current is extremely sensitive to the initial O_2 exposure dose.

One way of doing accurate measurements on the exposure dose is by doing the degradation experiments at low O_2 pressures (1.0×10^{-7} torr). This way we can have a better control on the degradation in emission current. In our experiment, we were able to monitor and record the O_2 partial pressure, get an online graph of the O_2 pressure versus time (P-t graph). In this way we can accurately calculate the exposure dose, which is the area under the P-t curve ($\int P(O_2)dt$).

The data obtained from these measurements permit estimation of the device lifetimes for coated and uncoated emitter tips, non-linearity of the degradation with duty cycle, change in emission area, average work-function and/or tip geometry.

REFERENCES

[1] C.A. Spindt and I. Brodie, Adv. Electron. Electron Phys. **83**, **1**, (1992).
[2] I. Brodie and P.R. Schwoebel, Proc. IEEE **82**, 1006 (1992).
[3] C.A. Spindt, J. Appl. Phys. **39**, 3504 (1968).
[4] L. Richter and R. Gomer, Surf. Sci. **83**, 93 (1979).
[5] W.A. Mackie, R.L. Hartman, M.A. Anderson and P.R. Davis, J. Vac. Sci. Technol. B **12**(2), 722 (1994).
[6] S. Meassick and H. Champaign, J. Vac. Sci. Technol. B **14**(3), 1914 (1996).
[7] B.R. Chalamala, Thesis (PhD.), University of North Texas 1996.
[8] H.M. Kennett and A.E. Lee, Surf. Sci. **48**, 591 (1975).
[9] E. Bauer and H. Poppa, Surf. Sci. **88**, 31 (1979).
[10] S. I. Castañeda, I. Montero, J.M. Ripalda, N. Díaz, L. Galan and F. Rueda, J. Appl. Phys. **85** (12), 8415 (1999).
[11] R. Gomer, *Field Emission and Field Ionization*, (Harvard University Press, Cambridge, MA, 1961).
[12] W.P. Dyke and W.W. Dolan, "Field Emission," Adv. Electronics and Electron Phys. **8**, 90, (1956).
[13] P.R. Schwoebel and I. Brodie, J. Vac. Sci. Technol. **B13**, 1391, (1995).
[14] T.A. Giorgi and P. della Porta, Eds., *Residual Gases in Electron Tubes*, (Academic Press, London, 1972).
[15] C.R.K. Marrian, G.A. Haas and A. Shih, Appl. Surf. Sci. **16**, 73, (1983).
[16] C.R.K. Marrian and A. Shih, IEEE Trans. Electron Dev. **ED-33**, 1874, (1986).
[17] G.A. Haas, R.E. Thomas, C.R.K. Marrian and A. Shih, IEEE Trans. Electron Dev. **ED-38**, 2244, (1991).
[18] B.R. Chalamala, R.M. Wallace, B.E. Gnade, J. Vac. Sci. Technol. **B16**, 2859 (1998).
[19] R.H. Fowler and L. Nordheim, "Electron emission in intense electric fields," Proc. Roy. Soc. London **119**, 683, (1928).
[20] J.H. Block in *Chemistry and Physics of Solid Surfaces*, edited by R. Vanselow and S.Y. Tong, (CRC Press, Boca Raton, FL, 1977), ch. **3**.
[21] C.A. Spindt, United States Patent: 4926056 (1990).
[22] P.H. Holloway, J. Sebastian, T. Trottier, H. Swart and R.O. Peterson, Solid State Technol. **38**, 47, (1995).
[23] C. Zhang, M. A. van Hove, and G. A. Somarjai, Surf. Sci. **149**, 326 (1985).
[24] G. H. Smuddle, Jr. and P. C. Stair, Surf. Sci. **317**, 65 (1994).
[25] Z. G. Liu, Y. Chen, and X. Z. Wen, Surf. Sci. **208**, L15 (1989).
[26] J. G. Choi and L. T. Thompson, Appl. Surf. Sci. **93**, 143 (1996).
[27] F. Okuyama, Surf. Sci. **67**, 109, (1977).

CHAPTER 2

FIELD EMISSION THEORY AND FIELD EMISSION MICROCATHODE ARRAYS

2.1. Introduction

The theory of electron emission from metals under the influence of strong electric fields has been applied in field electron and ion microscopy. Adsorption and desorption from surfaces, metal, and semiconductor interface studies have been performed by Gomer[1], Dyke and Dolan[2], Swanson and Bell[3] and Gadzuk and Plummer.[4]

Although field emission was first observed by R.W. Wood in 1897[5], theoretical predictions of the current - voltage characteristics were not particularly successful, since field emission was viewed as a classical process in which electrons were thermally activated and traversed a field reduced potential barrier.[6] A satisfactory theoretical explanation of field emission had to wait for the advent of quantum mechanics.

Using Schrödinger's wave theory, Fowler and Nordheim satisfactorily explained field emission as the quantum mechanical tunneling of electrons from the metal into vacuum under the influence of the applied electric field.[7] The now commonly referred to Fowler-Nordheim (F-N) equation, describes the relation between the emission current density J, the surface work function ?, and the applied electric field strength F.

2.2. Field Emission Theory

2.2.1 Field Emission

For electrons to escape from a metal surface, they need to have sufficient energy to overcome the potential barrier across the metal-vacuum interface. This quantity is

called the work function (?) and corresponds to the potential difference between the Fermi level (E_F) of the metal and the field free vacuum (E_v). Work function is a surface property of the material and depends on the electronic structure and orientation of the crystal plane. It differs for different crystallographic orientations of the same material. For example, crystalline Mo has reported work functions of 4.36 eV for the (112) face to 4.95 eV for the (110) crystallographic orientation.[8] The work function plays a dominant role in determining electron emission characteristics of metals.

The potential energy diagram of an electron at a distance x from the metal surface, with the applied field strength being F at the surface of the metal, is shown in Figure 2.1. The term $-e^2/4x$ arises from the attraction between the electron and the induced positive image charge on the metal, whereas -eFx is the potential on the electron, due to the applied electric field F, at the metal surface. Thus, the effective potential on the electron at a distance x from the surface with an applied electric field F at the surface is given by the equation:[9]

$V(x) = (E_F + ? - e^2/4x - eFx)$ for $x > x_c$ (2.1)

$V(x) = 0$ for $x < x_c$ (2.2)

where $x_c = e^2/[4(E_F + ? ?]$ such that $V(x_c) = 0$.

The applied electric field F lowers the potential barrier, and the effective barrier height can be obtained by setting $dV(x)/dx = 0$. The barrier reaches a maximum at a distance $x_l = (e/4F)^{1/2}$ from the metal surface, and this position is called the Schottky saddle point. In the presence of the field F, the maximum barrier height is reduced by [9]

$? ? = -(e^3F)^{1/2}$.

Thus the effective work function ϕ_{eff} can be written as

$$\phi_{eff} = \phi - e^{3/2} F^{1/2} \quad (2.3)$$

and this is called the Schottky effect. The barrier width at the Fermi energy level is

$$\Delta x = (\phi/eF) \quad (2.4)$$

if the image potential is not taken into consideration, and with the image potential taken into consideration, the barrier width is given by the following equation:

$$\Delta x = [(\phi/eF)^2 - 2/F]^{1/2} \quad (2.5)$$

For quantum mechanical tunneling of electrons to occur, the amplitude of the uncertainty in the position of the electron at E_F has to be comparable to the barrier width Δx from equation (2.5). The uncertainty in position (x) of the electron is related to the momentum (p) of the electron through the Heisenberg uncertainty relation

$\Delta x \cdot \Delta p = h/2\pi$ where h is Planck's constant. The uncertainty in the momentum of the electron at the barrier height ϕ is $\Delta p = (2m\phi)^{1/2}$ where m is the electron rest mass. Substituting $\Delta p = (2m\phi)^{1/2}$ in $\Delta x \cdot \Delta p = h/2\pi$, gives the uncertainty in position Δx:

$$\Delta x = h/(2\pi \cdot \Delta p) = h/[2\pi \cdot (2m\phi)^{1/2}] \quad (2.6)$$

For field emission to occur, the barrier width should be comparable or smaller than the uncertainty in the electron position Δx. This gives the field strength requirements for field emission to occur:

$$(\phi/eF) = h/[2\pi \cdot (2m\phi^2)^{1/2}]$$

or $$F = [4\pi (2m\phi^3)^{1/2}/eh] \quad (2.7)$$

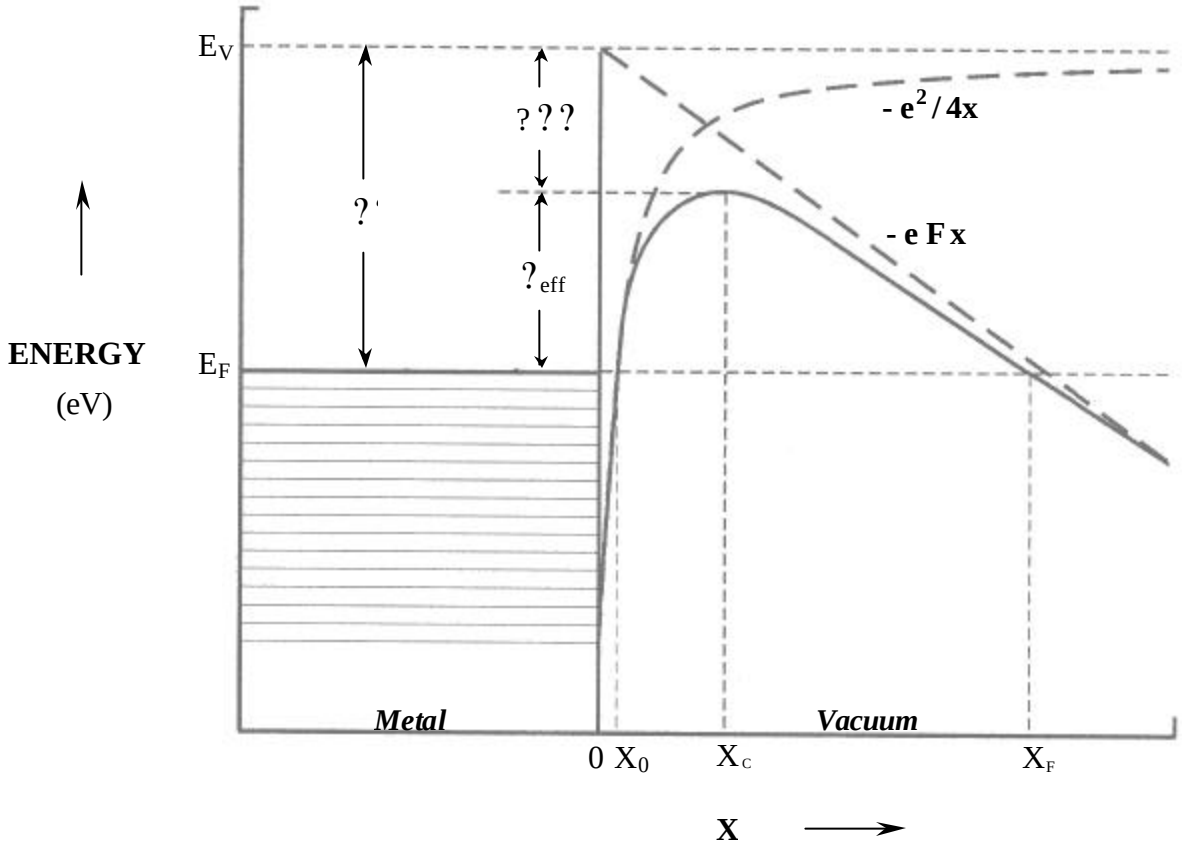

Figure 2.1 Potential energy diagram showing electron tunneling from a metal surface under the influence of an electric field.[10]

For metals with a surface work function of 4.5 eV, the width of the tunneling barrier ranges from 4.5nm at $3x10^7$ V/cm to 0.5nm at $3x10^8$ V/cm. Therefore for electric fields F > $3x10^7$ V/cm, appreciable tunneling is expected to occur.[1] The Fowler-Nordheim model for cold cathode field emission assumes that the metal has a uniform planar surface at 0K and that Fermi-Dirac statistics are valid for this problem. The number of electrons impinging on the surface barrier with normal energy between E and dE is given by:[11]

$$N(E,T)dE = (m\ d\ E / 2?^{2} l^{3}) \quad (2.8)$$

There is a probability D(E) of transmission of electrons through the surface potential barrier. The total current density (J_t) of the tunneling current is calculated by integrating P(E) over all the energy ranges;

$$J_t = e\ ?\ P(E)\ dE = e\ ?\ N(E,T)\ D(E)\ dE \quad (2.9)$$

The barrier penetration probability is obtained by solving the Schrödinger wave equation. After further calculations, the current density takes the form:[8]

$$J_t = [(1.56 \times 10^{-6}\ F^2)/(?\ t_y^2)] \times \exp\ [-6.44 \times 10^7\ f^{3/2}\ ?_y / F] \quad (2.10)$$

where J_t = current density in A/cm^2, F = field strength in V/cm, ? = surface work function of the metal in eV, $?_y$ is the Nordheim elliptic function that takes into account the image force and t_y another elliptic function which is almost equal to one.

2.2.2 Fowler-Nordheim Equation

The measured field emission current, I, is related to the current density J_t and the total area of the emitting surface A:

$$I = J_t\ A \quad (2.11)$$

The electric field strength F depends on the tip geometry and is given by

$$F = ?\ ?V \quad (2.12)$$

where ? is a geometric factor, which takes the emitter shape into account. Substituting, F and J_t in equation (2.10), one obtains the final form of the equation for field emission current:

$$I = [(1.56 \times 10^{-6}\ ?^{?}\ ?V^2\ A)/(?\ t_y^2)] \times \exp\ [-6.44 \times 10^7\ ?^{3/2}\ ?_y/(?\ ?V)] \quad (2.13)$$

This equation is referred to as the Fowler-Nordheim (F-N) equation. For metal field emitters, the plot of log (I/V^2) versus I/V gives a straight line and is called a Fowler-Nordheim plot. The slope of the line depends on the geometry and the surface work function of the metal. The y intercept depends on the emission area. The Fowler-Nordheim equation is generally written in a simpler form:

$$I = aV^2 \exp(-b\phi^{3/2}/V) \qquad (2.14)$$

where a and b are constants. Equation (2.14) can be re-written as:

$$\ln(I/V^2) = \ln a - b\phi^{3/2}/V \qquad (2.15)$$

which has the form of the equation of a line. This type of plot is called a Fowler – Nordheim plot. A change in the slope of the line indicates either a change in the work function, or in the geometry of the tip or both. Thus a change in work function or tip geometry cannot be independently isolated. It has been reported that, for small nominal gaseous exposure doses there is no significant change in tip geometry.[10] In this case, the change in slope is due to the change in work function. The slope (m) of the F-N plot is proportional to $\phi^{3/2}$.

The dependence of the slope of the F-N plot on the work function has been used to measure relative changes in the work function resulting from surface modifications, and to study adsorption and desorption kinetics of gases on clean metal surfaces.[3]

2.2.3 Selection of Tip Materials

Field emitter tip materials should have a low work function as well as good electrical and mechanical properties. The tips should be capable of withstanding extremely high electrical stresses. The material should also be well suited for processing

using standard micro fabrication technologies. Apart from the surface work function (?) of the material, geometric factors, like the aspect ratio, play a significant part in determining the emission characteristics. The need for creating emitter tips with high aspect ratios imposes critical requirements on materials that could be used as field emitter cathodes.

It is hard to find one material, which satisfies all the above requirements. For example, group I and II metals have a low work function, but they are chemically reactive and are not suitable for making high aspect ratio structures.[12] Group I B elements like Ag and Au have excellent electrical properties, but have a higher work function and poor mechanical properties. Rare earths and transition metals are inert, mechanically strong and have the highest reported melting points. Thus W, Mo, Zr and Ir are some of the most commonly used thermionic and field emitter materials.[13] Table 2.1 lists the relevant electrical, electronic and thermal parameters for important rare earth, transition and noble metals.

The aspect ratio (height/bottom diameter of the cone) of the emitters is an important factor in determining the emission characteristics. A higher aspect ratio results in a substantial decrease in the required gate voltage for the same emission current. Itoh, *et al*, measured the aspect ratios that can be achieved with different metals in a Spindt type field emitter geometry. The reported aspect ratios for Mo, Ti, Nb, Zr and Cr are 1.3, 0.5, 2.0, 0.8-0.9 and 1.43 respectively.[12]

Metal	**Work Function** ? ? (eV)	**Melting Point** T_M (°C)	**Resistivity** ? ??? ?(x 10^{-8} ? -m)	**Thermal Conductivity** K_{300} (W/cm-K)
Titanium	4.33	1668	39.00	0.219
Zirconium	4.05	1855	38.80	0.227
Niobium	4.30	2477	15.20	0.537
Chromium	4.50	1907	11.80	0.937
Molybdenum	4.60	2623	4.85	1.380
Tungsten	4.55	3422	4.82	1.740
Rhenium	4.96	3186	17.20	0.479
Ruthenium	4.98	2334	7.10	1.170
Iridium	5.27	2446	4.70	1.470
Nickel	5.15	1455	6.16	0.907
Palladium	5.12	1555	9.78	0.718
Platinum	5.65	1768	10.50	0.716

Table 2.1 Summary of thermo-physical, electronic, and work function data for common rare earth, transition metal and noble field emitter materials. The work function for polycrystalline metals was adopted from the work-function compilation of Michaelson.[14] The thermo-physical data was taken from the CRC Handbook of Physics and Chemistry.[15]

The data in Table 2.1, and the measured aspect ratio, indicate that Mo, Nb and Cr are preferred candidates. For historical and manufacturing reasons, Mo has been the material of choice for the production of most field emitter arrays.

There are serious disadvantages in using metals in elemental form. Frequently, pure metals like Mo are susceptible to oxidation by residual gases like O_2, H_2O, CO_2 and CO present in the vacuum envelope.[16] To prevent the oxidation of the tips, several

alternate materials are being studied in laboratories around the world. Refractory carbides have lower work function than the refractory metals and are less susceptible to surface contamination by oxygen containing species.[17,18] Attempts have also been made to deposit thin films of diamond on the Mo FEAs.[19,20,2122,23]

2.3. Spindt type Field Emission Micro-cathode arrays

Until recently, the use of field emitter tips was limited to applications in field electron and ion microscopes. Currently, there is a growing interest in the development of vacuum microelectronic devices and technologies based on large arrays of field emitter cathodes. Creation of large field emitter cathode arrays (FEAs) has been made possible with Spindt's deposition process for the fabrication tips.[24] This breakthrough made it possible to create large field emitters arrays using common micro-fabrication technology employed in the electronics industry.

The integration of field emitters and advanced microelectronic technologies make it possible to create FEA vacuum microelectronic devices. The high current density, low power requirements, and the ultra high speed switching that can be accomplished with ballistic electrons makes these devices suitable candidates in high resolution displays and high speed RF applications.[25,26]

Utsumi presented a comparative analysis of the field emitter vacuum microelectronics and silicon based semiconductor technology.[27] The major advantages of vacuum microelectronic devices include ultra high-speed switching, higher power output, large operating temperature range and beam focusing and deflection capabilities. The major obstacle is the requirement of a high vacuum in the device. Other vacuum related

problems are emission current instabilities and device failures resulting from the contamination of the emitter tips by the residual gases in the vacuum package.

The arrays studied in this work were made by Pixtech for Texas Instruments. The performance of similar devices has been reported in the literature. Figure 2.2 shows a scanning electron microscope (SEM) image of a section of the field emitter array.

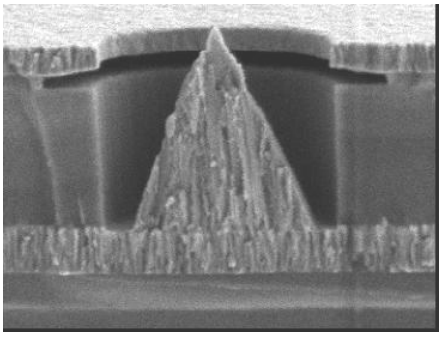

Figure 2.2 SEM image of a section of the Spindt type FEA.[28]

The Mo tips are positioned atop a resistive layer of amorphous silicon for limiting the emission current from each tip and to avoid catastrophic failures resulting from runaway current. A thin layer of niobium metal deposited on top of the SiO_2 gate dielectric serves as the gate electrode. For the FEAs studied in this work, the gate elements are tied to a single external electrode.

2.4. Emission Characteristics

The current-voltage (I-V) characteristics of a Spindt type FEA (#32107) are shown in Fig 2.3. A positive bias (V_g) is applied between the Mo cathode and the gate electrode and the field-emitted electrons leaving the array are collected on a platinum coated silicon wafer, which works as the anode. The potential on the anode was kept at +400 V (for DC mode) or +320 V (for Pulsed mode) with respect to the cathode.

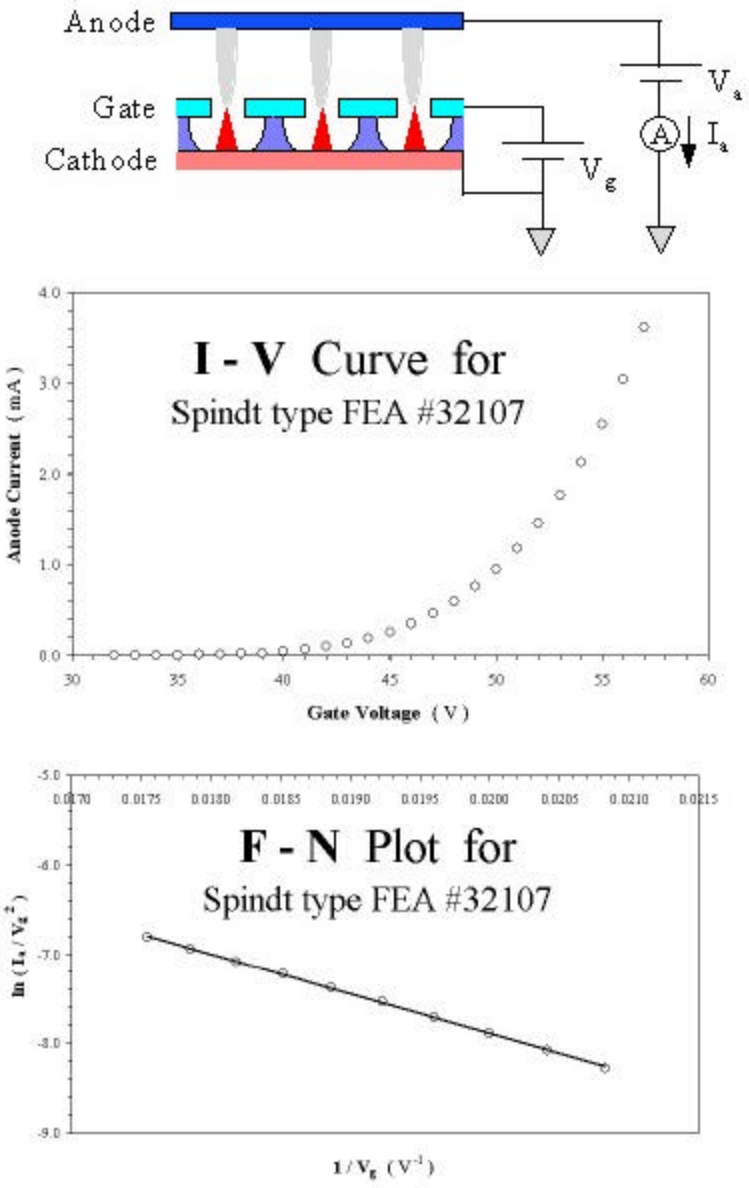

Figure 2.3 I-V and F-N plots for Spindt type FEA # 32107

For all the FEAs characterized, the gate voltage threshold for measurable field emission current was between 35 - 55 V. The peak emission current was approximately 50 mA at a gate voltage of 75 V for Mo FEAs and around 85-90V for Au coated FEAs.

2.5. Application of the Fowler-Nordheim Theory to FEAs

For a simple field emitter, the relation between the gate voltage V and emission current I is given by the Fowler-Nordheim (F-N) equation:

$$I = aV^2 \exp(-b\phi^{3/2}/V) \quad (2.16)$$

Although the above equation is true only for a single emitter tip, it can be applied to a FEA with millions of emitting tips. The reason being that the number of emitting tips is more or less a constant (from the I-V and straight line fit for the F-N data). The primary difference is that the solution of the F-N equation provides the average work function of the emitter tips and the total emission area.

If the work function of the clean surface is known, the modified work function (ϕ_d) after gaseous exposures would be $\phi_d = (m_d / m_c)^{2/3} \phi_c$ where m_c and m_d are the slopes of the F-N plot, for the clean and modified field emitter respectively.

2.6. Standardization of Field Emission Results[29]

Many problems with interpretation of FE results arise from the substitution of the Fowler-Nordheim (FN) equation (2.17), which links local emission current density J from a field emission source with the work function ϕ and the local applied electric field F:

$$J(F) = (AF^2 / \phi t^2) \exp(-B \phi^{3/2} / F) \quad (2.17)$$

[$A = 1.54\times10^{-6}$ A eV / V^2, $B = 6.83\times10^{7}$ $eV^{-3/2}$ Vcm^{-1}] with an experimentally adapted equation (2.18), showing the measurable characteristics, current (I) and voltage (V):

$$I(V) = aV^2 \exp(-b/V) \quad (2.18)$$

where a and b are experimentally derived factors. I can be converted to J, and V to F by linear factors:

$J = I/\beta$ (2.19)

$F = \beta V$ or $F = \beta\gamma F_0$ (2.20)

$F_0 = V/d$, where α is the emission area, β is the field factor (local field to voltage ratio), γ is the field enhancement factor, and d is the planar anode to planar cathode distance. This is only true for a diode configuration. It is worth noting that the literature uses β for both F/V and F/F_0 quantities, which is immediately confusing.

Clearly, the correct determination of α and β are critical for purposes of interpretation and comparison of experimental FE results from various conditions. Different experimental arrangements present different problems in this regard, and this makes quantitative comparisons difficult.

2.6.1 Low emission threshold and low work function

The actual work function is about 5eV for most available (stable) materials. The apparent work function is the value from the slope of the FN plot. As follows from equations (2.17) and (2.18), the apparent work function in Eq. (2.18) is connected to the actual work function in Eq. (2.17) through the ratio of assumed and actual value of β:

$\phi_{apparent} = (\beta_{assumed} / \beta_{actual})^{2/3} \phi_{actual}$ (2.21)

The effective work function is used in the case where emission characteristics of an emitter are compared to a reference emitter with a well-defined β (for example, metal tips before and after cold deposition of a coating). The effective work function reflects the shift of the current-voltage (I-V) characteristics relative to a reference curve, e.g., as an effect of coating. Another source of misinterpretation is relying upon the FN emission law and ignoring other possible mechanisms contributing to emission. A classic example

is the low-field cold emission observations reported in the 1960s for MgO films[30], suggesting a work function of 0.01 eV based on analysis using the FN equation. It was found that internal secondary emission from a porous MgO film was primarily responsible for the observed phenomenon.

2.6.2 High current density

The determination (and definition) of ? is also critical in the interpretation of FE field emission experiments. The basic FN equation has been obtained for the local current density, J, and considers uniform emission from an arbitrary planar area. This is what we call the theoretical (or physical) current density.

One of the ways to derive ? is from the intercept of a FN plot,[25] which is typically referred to as the FN area denoted as $?_{FN,}$ where $?_{FN}$ = exp(a). Typically, this method gives the value of the effective size of emission area (e.g., $?_{FN}^{1/2}$), about 1-10% of the physical tip radius in the range of 10-100 nm.[25]

Therefore, using the FN area to calculate the current densities, even very small emission currents, would result in very high current densities. The relationship between the FN area and the actual emission area is still uncertain. The term "Field Emission Area" must be clarified in order to make it a useful value for experimentalists. An important step in this direction is a new procedure proposed by Forbes for the derivation of emission area from FN plots.[31] Another popular definition of emission area is the physical area of the emitting tip of radius r, where we have $?_{tip} = r^2$, which also results in a high current density.

There are two main categories of real area, namely “true area of emission” (assuming emission is uniform) and “macroscopic area”. The simplest one is derived using the FN equation (by extending the F-N plot, back to the y axis). The figure of merit for device applications is the integral current density, i.e., the total current emitted divided by the entire cathode area.

The integral current density depends upon cathode area. A very high current density is obtained only from a very small cathode area. The record current density of 2000 A/cm^2, was obtained from an array of emitters with an integral area of approximately 20 $?m^2$ and a total current of a few mA.[25]

2.7. Characteristics of Emitters – Fabrication History

The interpretation of the emission data depends strongly on the emitter material and fabrication history. However, we briefly formulate the questions to be addressed in any publication on the above subject. How was the material fabricated (in detail)? What is its composition? How thick is the film (or does it vary in thickness) or what size (distribution) are the particles? How smooth (rough) is the surface? What are the minor constituents (dopants, defects)? Without these data, a working theory applicable to device application will be nearly impossible.

2.8. Details of Experimental Procedure

2.8.1 Vacuum

There is a high probability that a cathode well behaved in UHV conditions will show much worse performance in a practical device environment. On the other hand,

experiments performed in environments that are not ultrahigh vacuum appear to be less reliable from the point of view of physical insight.

2.8.2 Emission stability

1. *Low frequency current fluctuation (short-term stability)*

   In order to measure the low-frequency current fluctuations, the value of ?? = $(I_{max}-I_{min})/I_{av}$ can be used, where I_{max}, I_{min} and I_{av} correspond to the maximum, minimum, and average values of current within a measurement cycle.

2. *Long-term stability*

   Long-term stability can be characterized as the $I_{av}(t)$ plot during long periods of time (e.g., tens, hundreds, and thousands of hours). It is highly desired, after the long-term stability test, to investigate both the cathode and anode for morphological and compositional changes.

2.8.3 Reproducibility of I-V characteristics

Another important practical characteristic is the reproducibility of the I-V plots with time and repeated increase/decrease of applied voltage. Sometimes field emitters demonstrate hysteresis, which is an undesirable property for practical applications. At the same time, hysteresis can provide information about the emission mechanism. For reliable results, all measurements should be performed after a period of "conditioning", i.e., the process by which the voltage is ramped up and down repeatedly until reproducible emission characteristics are observed.

REFERENCES

[1] R. Gomer, Field Emission and Field Ionization, Harvard Univ. Press, Cambridge, MA, 1961.
[2] W.P. Dyke and W.W. Dolan, Adv. Electron. Electron Phys. **8**, 90, (1956).
[3] L.W. Swanson and A.E. Bell, Adv. Electron. Electron Phys. **32**, 193, (1973).
[4] J.W. Gadzuk and E.W. Plummer, Rev. Mod. Phys. **44**, 487, (1973).
[5] R.W. Wood, Phys. Rev. **5**, 1, (1897).
[6] R.A. Millikan and C.F. Frying, Phys. Rev. **27**, 51, (1926).
[7] R. H. Fowler and L.W. Nordheim, Proc. Roy. Soc. London **A119**, 173, (1928).
[8] S. Berge, P.O. Gartland and B.J. Slagvold, Surf. Sci. **43**, 275, (1974).
[9] V.T. Binh, N. Garcia, S.T. Purcell, Adv. Imaging and Electron Physics, **95**, 74 (1996).
[10] B.R. Chalamala, Thesis (PhD.), University of North Texas 1996.
[11] A. Modinos, *Field, Thermionic and Secondary Electron Emission Spectroscopy*, Plemum Press, New York, 1-18 (1986)
[12] S. Itoh, T. Watanabe, K. Ohtsu, M. Taniguchi, S. Uzawa and N. Nishimura, J. Vac. Sci. Technol. **B13**, 487, (1995).
[13] V.E. Hughes and H.L. Schultz, Meth. Exper. Phys. **4**,1, (1967).
[14] H.B. Michaelson, J. Appl. Phys. **48**, 4729, (1977).
[15] D.R. Lide, ed., CRC Handbook of Physics and Chemistry, (Boca Raton, FL: CRC Press, 1996).
[16] P.R. Schwoebel and I. Brodie, J. Vac. Sci. Technol. **B13**, 1391, (1995).
[17] W.A. Mackie, C.L. Hinrichs and P.R. Davis, IEEE Trans. Electron Dev. **ED36**, 2687, (1989).
[18] W.A. Mackie, T. Xie, and P.R. Davis, J. Vac. Sci. Technol. **B17**, 613 (1999).
[19] W.B. Choi, J. Lin, M.T. McClure, A.F. Myers, V.V. Zhirnov, J.J. Cuomo and J. Hren, J. Vac. Sci. Technol. **B14**, 2050, (1996).
[20] J.H. Jung, B.K. Ju, Y.H. Lee, J. Jang, and M.H. Oh, J. Vac. Sci. Technol. **B17**, 486, (1999).
[21] J.H. Jung, B.K. Ju, H. Kim, M.H. Oh, S.J. Chung, and J. Jang, J. Vac. Sci. Technol. **B16**, 705, (1998).
[22] M.T. McClure, R. Schlesser, B.L. McCarson, and Z. Sitar, J. Vac. Sci. Technol. **B15**, 2067 (1997).
[23] Z. X. Yu, S.S. Wu and N.S. Xu, J. Vac. Sci. Technol. **B17**, 562 (1999).
[24] C.A. Spindt, J. Appl. Phys. **39**, 3504, (1968).
[25] C.A. Spindt and I. Brodie, Adv. Electron. Electron Phys. **83**, 1, (1992).
[26] I. Brodie and P.R. Schwoebel, Proc. IEEE **82**, 1006 (1992).
[27] T. Utsumi, J. Soc. Infor. Displ. **1/3**, 313, (1993).
[28] B.E. Gnade, "The Evolution of Flat Panel Cathode Ray Tubes", 3 (2001).
[29] V.V. Zhirnov, J. Vac. Sci. Technol. **B19**, 87 (2001).
[30] W.M. Feist, Adv. Electron. Electron Phys., Suppl. **4**, 1 (1968).
[31] R.G. Forbes, J. Vac. Sci. Technol. **B17**, 526 (1999).

CHAPTER 3

EXPERIMENTAL SETUP AND INSTRUMENTATION

3.1. Introduction

In this chapter, the experimental setup and measurement electronics are presented. The effect of O_2 exposures on Au coated field emission arrays (FEAs) was examined by studying the degradation in anode current for Au coated arrays and comparing them to the results obtained for uncoated arrays.

3.2. Gas Exposures on FEAs – Emission Studies[1]

The UHV system shown in Figure 3.1 consists of a Perkin-Elmer TNB-X/1000 ultra high vacuum (UHV) analytical chamber equipped with an ion pump and a titanium sublimation pump. A turbo molecular pump was used for initial pump down to the UHV range. After a 24-hour bake out at 100 °C, a base pressure of 8×10^{-9} torr was attained.

This low operational base pressure assures control of the residual species for the field emission array ambient. A sapphire sealed variable leak valve was used for introducing the gases into the system. The total pressure in the system was measured using a UHV nude ionization gauge. This permitted control of gas partial pressures from 1×10^{-8} to 2×10^{-6} torr.

The field emitter array is mounted on a FEA holder, which has a provision for attaching an anode. The spacing between the cathode and anode is 1 cm and the terminals are electrically isolated. The cathode is grounded while the gate electrode is positively biased for field emission.

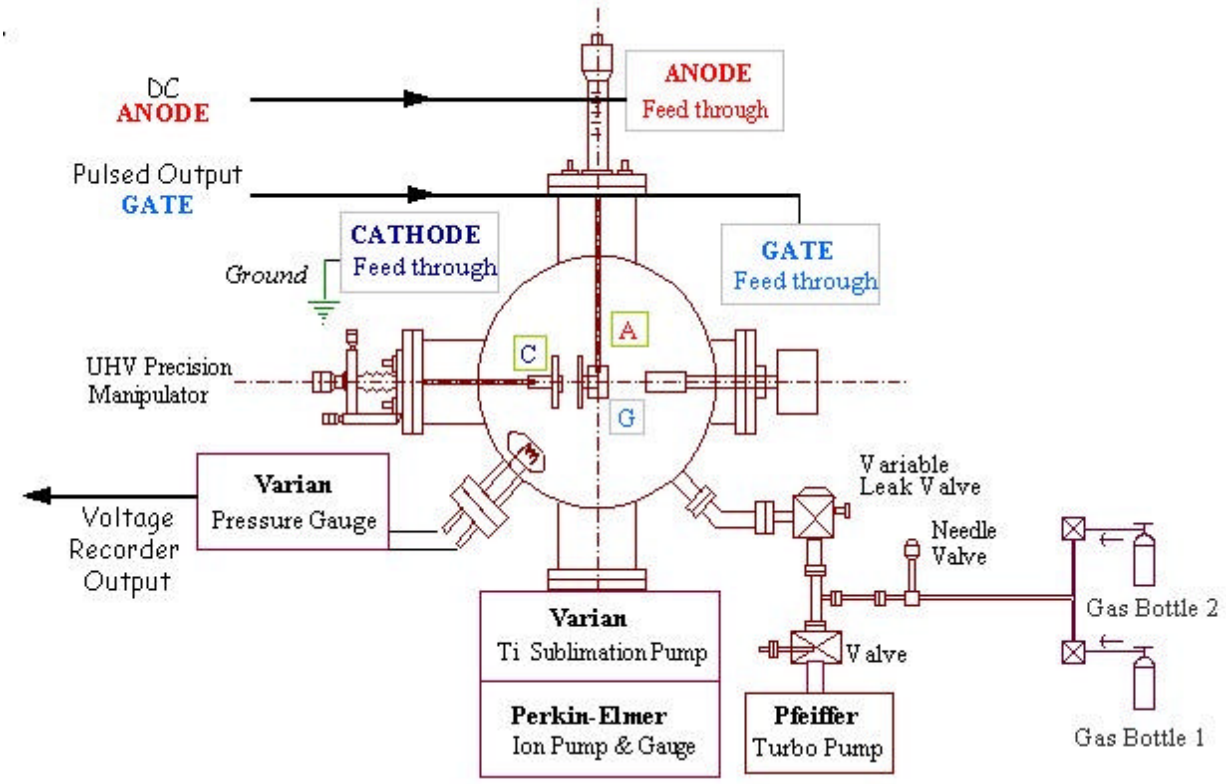

Figure 3.1 Schematic layout of the experimental apparatus for studying the effects of gas exposures on active field emitter arrays.[1]

The effects of contamination of the cathode array from anodes coated with cathodoluminescent or metal-oxides have been reported.[2] To avoid such spurious effects, the emitted electrons in this study are collected on an inert platinum coated silicon anode. The gate to cathode potential (V_g) and the anode current (I_a) are monitored throughout each experiment.

The instrumentation and data acquisition electronics setup are shown in Figure 3.2. The power supplies and measurement electronic devices, equipped with the IEEE-488 interface are connected to a personal computer with a GPIB (IEEE-488) card. Automated data acquisition and control is accomplished with Labview 6.0i software,[3]

which uses the IEEE-488 interface bus. Labview is a user-friendly graphical program with the ability to control and read data from up to 14 instruments.

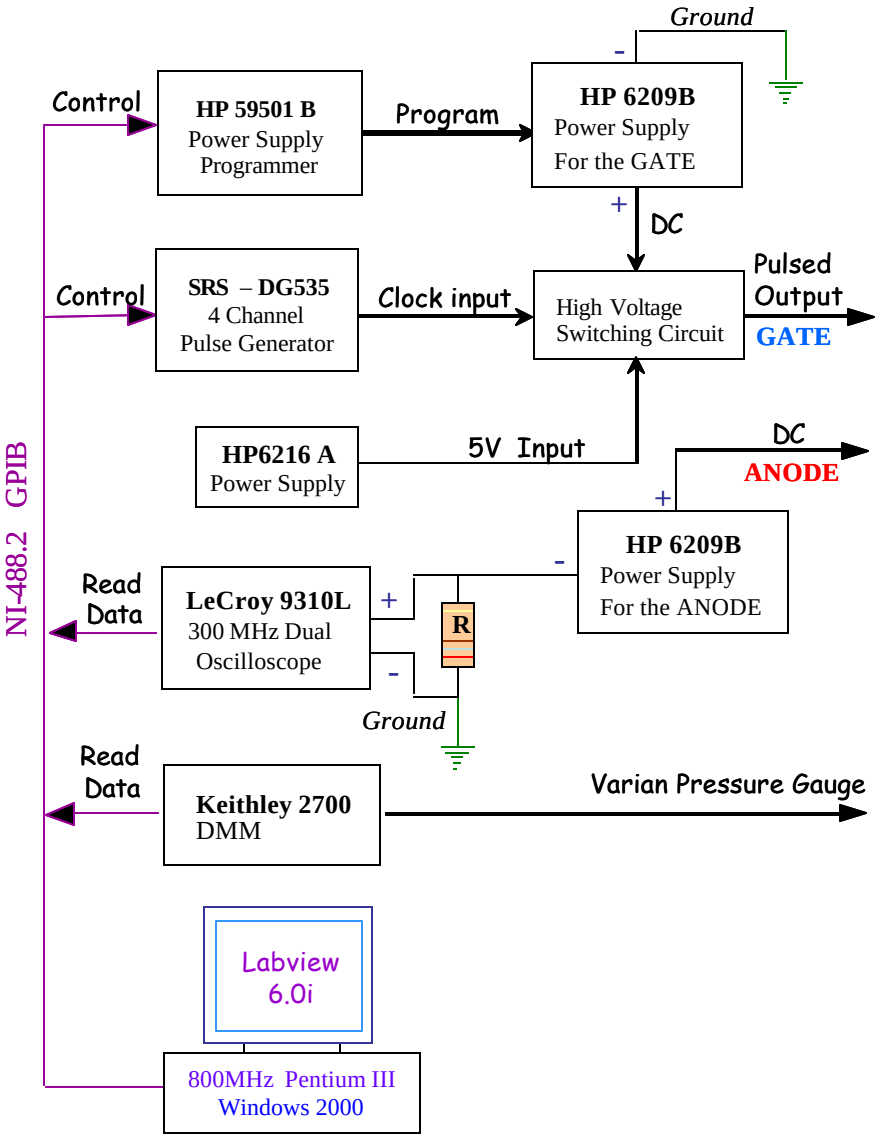

Figure 3.2 Schematic of the instrumentation and data acquisition electronics setup used for measuring the effects of gas exposures on active FEAs.[1]

3.3. Electrical Connections

3.3.1 Gate Power Supply & Programmer

The circuit diagram in Fig 3.2 shows the HP 59501B[4] power supply programmer as a controller for the HP 6209B[5] DC power supply. The HP 59501B is controlled by the GPIB interface and an output voltage signal (0 – 10V) is sent to the HP 6209B power supply, which is amplified to get the output gate voltage (0-100V).

The amplification, or gain, is determined by the value of the resistors used. For all our experiments, R_P = 10k? and R_R = 1k? . This gives a gain of about 10 and a range of approximately 0 – 100V. The HP 59501B voltage programmer and HP 6209B power supply were calibrated (see appendix) and tested for the output voltage. The accuracy of the power supply was approximately 0.5%, so the error in voltage was less than 0.5V up to 100V.

Voltage Gain:

?

$? = V_{Output} / V_{Intput} = R_p / R_R = 10$

HP59501B Power Supply Programmer :

Output Range is 0 – 10 V DC

HP6209B Power Supply :

Output Range is 0 – 100 V DC (Limited by the Gain of the above Setup)

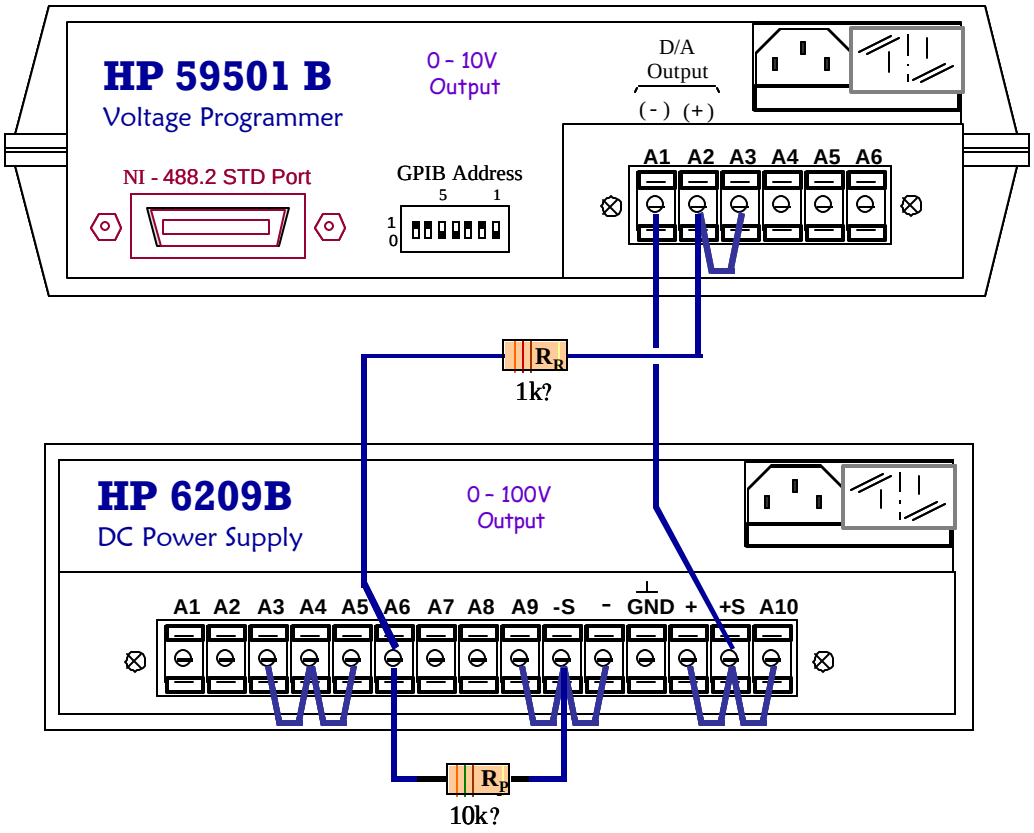

Figure 3.3 Schematic and wiring diagram of the HP59501B power supply programmer to the HP6209B DC power supply.[4,5]

3.3.2 Anode Power Supply, Programmable Pulse Generator & Oscilloscope

A 330? resistor was connected as shown in Fig 3.2. The voltage pulse was measured across the ends of the resistor. The anode current was calculated by dividing the voltage (oscilloscope) by 330. There was some reduction in the total anode current due to the resistor, but it can be neglected as it is less than 1%. The anode voltage was kept constant at 300V with respect to the cathode.

In the pulsed mode of operation, the gate voltage, V_g, was switched on and off at the desired rate (duty cycle) using a high speed switching circuit (Figure 3.4). A

programmable pulse generator SRS DG-535[6] provides the necessary control signals to the high speed switching circuit, whose output modulates between 0 and V_g. The anode current waveform measurements were performed using a Lecroy 9310 digital oscilloscope.

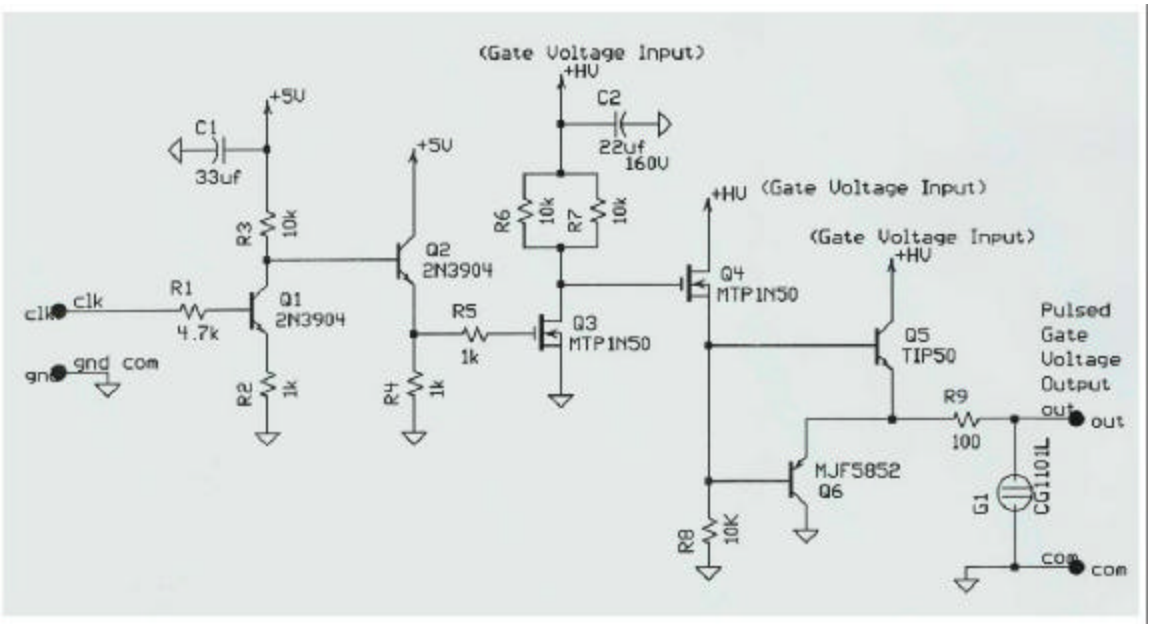

Figure 3.4 A high speed switching circuit designed for the pulsed mode operation

An example of the voltage pulse measured by the oscilloscope is shown in Figure 3.5. Each square represents 50?s (X - time) and 0.64V (Y – voltage). The pulse shown below is not a perfect square wave and has a rise time of approximately 28?s, an ON time of approximately 20ms and a fall time of 2?s.

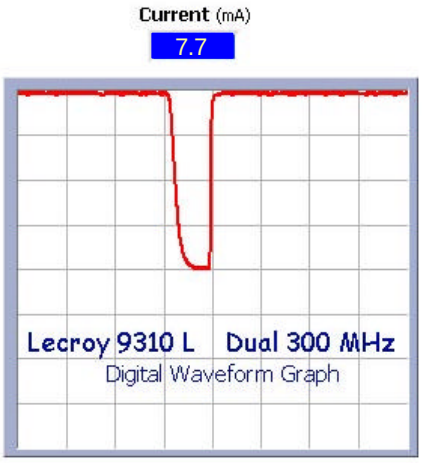

Figure 3.5 Waveform graph showing the 50?s Anode Current pulse at 0.5% Duty Cycle

3.4. Evaporation

3.4.1 Introduction

The schematic of the evaporator system used is shown in Fig 3.6. The film thickness calibration is done by depositing Au on a (100) Si sample for different periods of time. The temperature of the evaporation cell is set to 1300°C, and the time varies between 10 - 30 minutes (depending upon the desired Au thickness). After deposition, the film thickness is determined using RBS (Rutherford Back Scattering). Once the RBS thickness (?g/cm^2) is determined, the physical thickness (Å) can easily be calculated using the film density (g/cm^3).

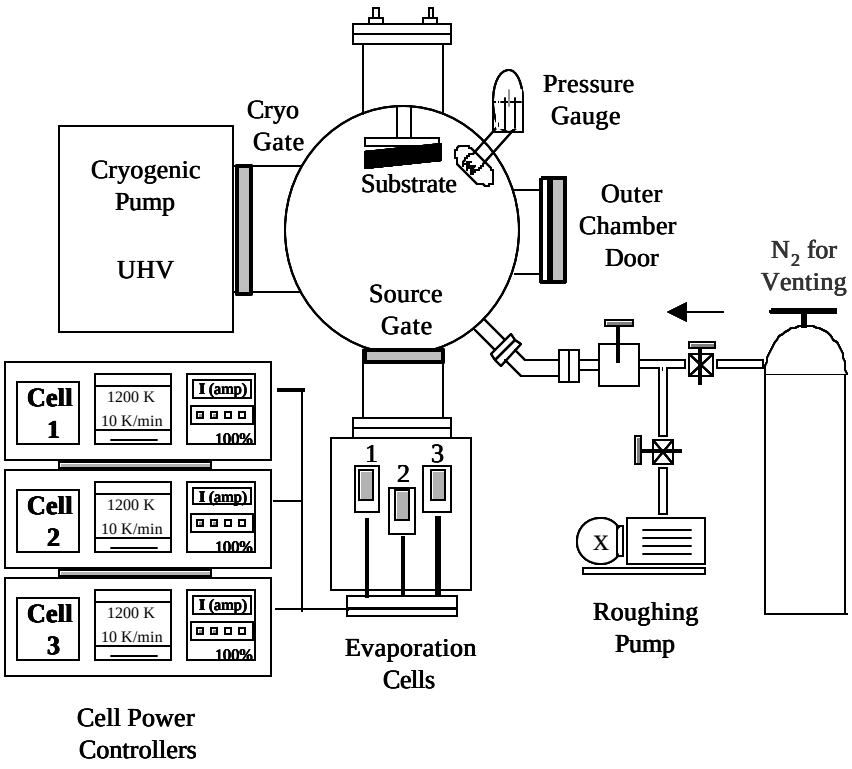

Figure 3.6 Schematic of the Evaporation System with CTI Cryo-pump and Radak Power controller for 3 evaporation cells.

3.4.2 Evaporation Theory

The thickness of the evaporated film is a function of the vapor pressure and the sticking coefficient (metal-substrate). For the same metal film (Au), the film thickness is proportional to the deposition time and vapor pressure, which is a function of the cell temperature. The temperature - vapor pressure curve for Au[7] is shown in Figure 3.7.

At a temperature of 1300°C, the vapor pressure of Au is about 2.2 $\times 10^{-3}$ torr

providing a deposition rate of 3Å/min. The primary equation, which relates the incident flux (***F***) to the pressure (**P**) of the metal vapor and temperature (***T***), is:[8]

$$\boldsymbol{F} = \boldsymbol{P} / (2 \pi m k \boldsymbol{T})^{0.5} \qquad (3.1)$$

Where, the units of ***F*** are molecules/m^{2}s, ***P*** in torr and ***T*** in K

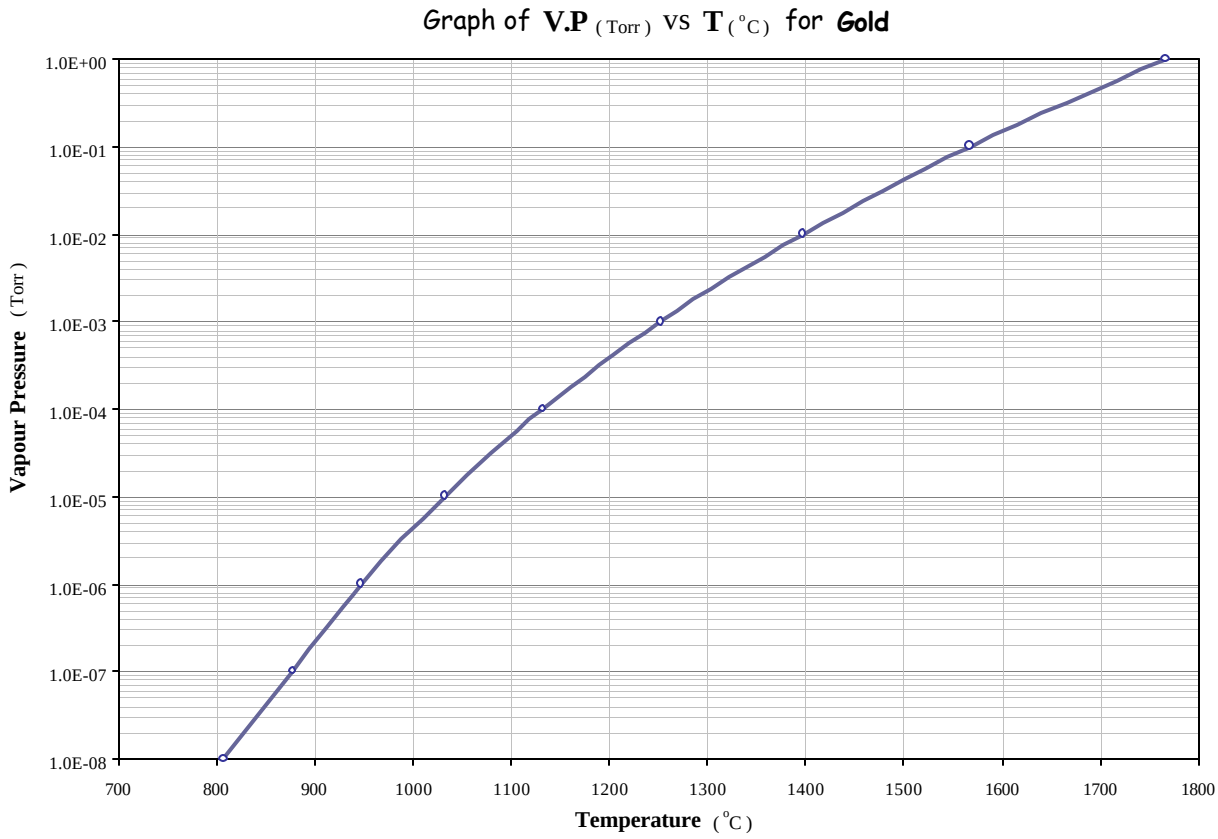

Figure 3.7 Graph showing the vapor pressure (torr) of Au versus temperature (°C). The vapor pressure is plotted on a logarithmic scale.[7]

The minimum estimate for the time to deposit a monolayer of metal film on a clean surface (assuming a unit sticking probability i.e. S = 1) is shown below. The monolayer coverage is generally on the order of 10^{15} /cm^2. We now have

$$\mathbf{t} = (10^{19} / \boldsymbol{F}) \qquad (3.2)$$

where,

t = Time to deposit a single atomic layer

F = Incident Flux (molecules/m^2s)

The deposition rate (Å/min), is calculated knowing the molecular density (atoms/cm^3).

3.4.3 Coating Field Emitter Arrays with Au

The FEA to be coated is first cleaned using an ultrasonic cleaner. This should be done to remove any small particulates attached to the Mo surface and also to reduce any electrical shorts between the gate and cathode columns. After the array has been cleaned, it is removed and dried with N_2 to evaporate the isopropanol from the FEA surface. The FEA is then securely attached to a shadow mask, which includes a spectator sample. The shadow mask ensures that the Au is deposited only within the emission area so as to not create an electrical short between the gate and cathode (Figure 3.8). The thickness of the deposited gold layer is determined by the deposition rate and time.

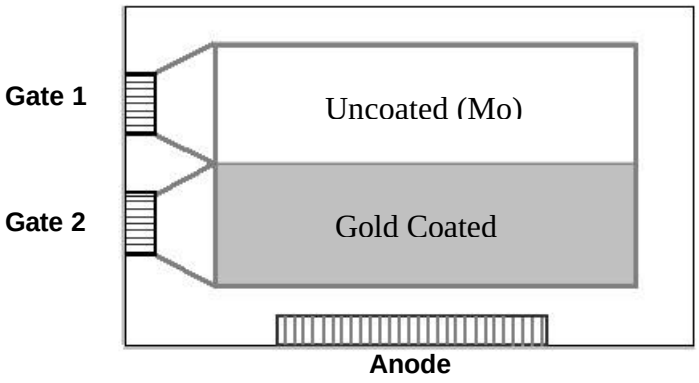

Figure 3.8 An FEA coated with Au on half the area.

The actual thickness of Au deposited on the cone, will not be the same as the gold thickness on a flat surface spectator sample (Figure 3.9). The relation between the Au film thickness deposited on the Mo cone and that deposited on the flat surface of the spectator sample is presented in equation (3.3).

$$d_a / d = (\text{Base Area of Cone} / \text{Curved Area of Cone}) \quad (3.3)$$

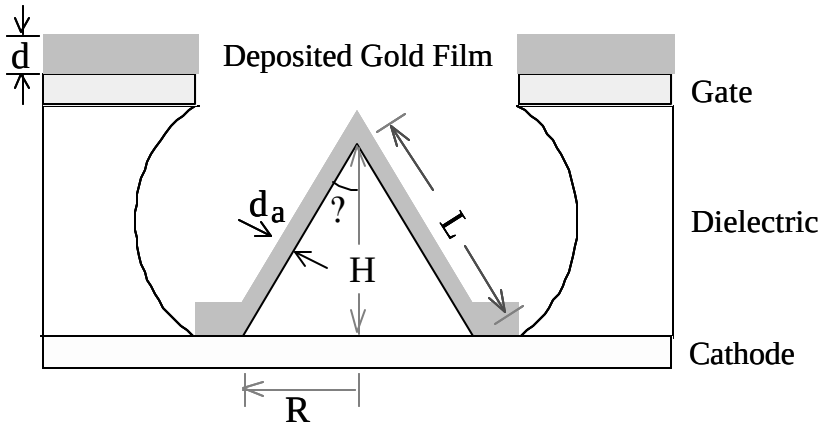

Aspect Ratio (??) = 2R/H = 1.2

Tan ?? = R/H = ?/2 = 0.6

?? = 30.96°

R/L = Sin ?? = 0.515

Figure 3.9 Diagram showing the section of a field emitter tip, coated with Au. The Au thickness on the gate (flat surface) and on the emitter tip is related to its aspect ratio.

Unless specified, the Au film thickness listed below is the thickness on the spectator sample, as determined by RBS. We coated six FEAs with Au films of different thickness. Out of these, only two FEAs had half their emission area coated with Au and the other half was left uncoated.

REFERENCES

[1] B.R. Chalamala, Thesis (PhD.), University of North Texas 1996.
[2] P.H. Holloway, T.A. Trottier, J. Sebastian, S. Jones, X.M. Zhang, J.S. Bang, B. Abrams,W.J. Thomes, and T.J. Kim, J. Appl. Phys. **88**, 483, (2000)
[3] Labview^{TM} 6.0i is a registered trademark of National Instruments Inc., Austin, Texas (2000).
[4] HP 59501B Power Supply Programmer Manual.
[5] HP 6209B DC Power Supply Manual.
[6] Stanford Research Systems, Inc., 1290-D Reamwood Avenue, Sunnyvale, CA 94089.
[7] R.E. Honig, and D.A. Kramer, *Vapor Pressure Data for the Solid and Liquid Elements,* RCA Review **30**, 285-305, (1969).
[8] J.M. Lafferty, *Foundations of Vacuum Science and Technology*, Microelectronics Journal, **31**, 2, (2000).

CHAPTER 4

DEGRADATION OF FIELD EMITTER ARRAYS

4.1. Introduction

In this chapter, the results of the experimental measurements on the O_2 degradation of active Mo FEAs are presented. From the Fowler-Nordheim (F-N) curves, before and after degradation, the relative changes in the slope and y - intercept were calculated. B.R. Chalamala *et al*. has reported the degradation in emission current due to O_2 exposures on Spindt type FEAs.[1] O_2 is present within the device envelope and readily interacts with Mo forming Mo oxides.

Emission degradation of the field emission cathodes can occur in many ways. Adsorption of gases on the tip surface can result in a work function change, thereby changing the emission. High field-induced chemical reactions also play an important role in determining the surface chemistry and physics of these devices during their operation.[1]

In a typical Spindt cathode array, the gate to tip spacing is about 0.5?m. For gate voltages of 50-100V, electric fields as high as 10^8 V/m can be achieved near the tips. With such high fields, field dissociation of gases can occur near the emitter surface. The resulting ions and free radicals can further modify the surface of the tips and change the work function and therefore the emission current.[1]

4.2. FEA Activation - Tip Conditioning

The FEAs are activated (i.e. run for several hours at a constant current), using a simple Current controller created in Labview 6.0i[2] (see Appendix). A screen view of a tip conditioning experiment is shown in Figure 4.1.

4.2.1 Tip Conditioning at constant Current

Initially the FEAs required a high gate voltage (80V) to start emitting. By applying a voltage, there is some tip cleaning due to field desorption and removal of the oxide layer, which results in an increase in emission current for the same voltage. However, too much emission current from the tips changes the tip geometry.

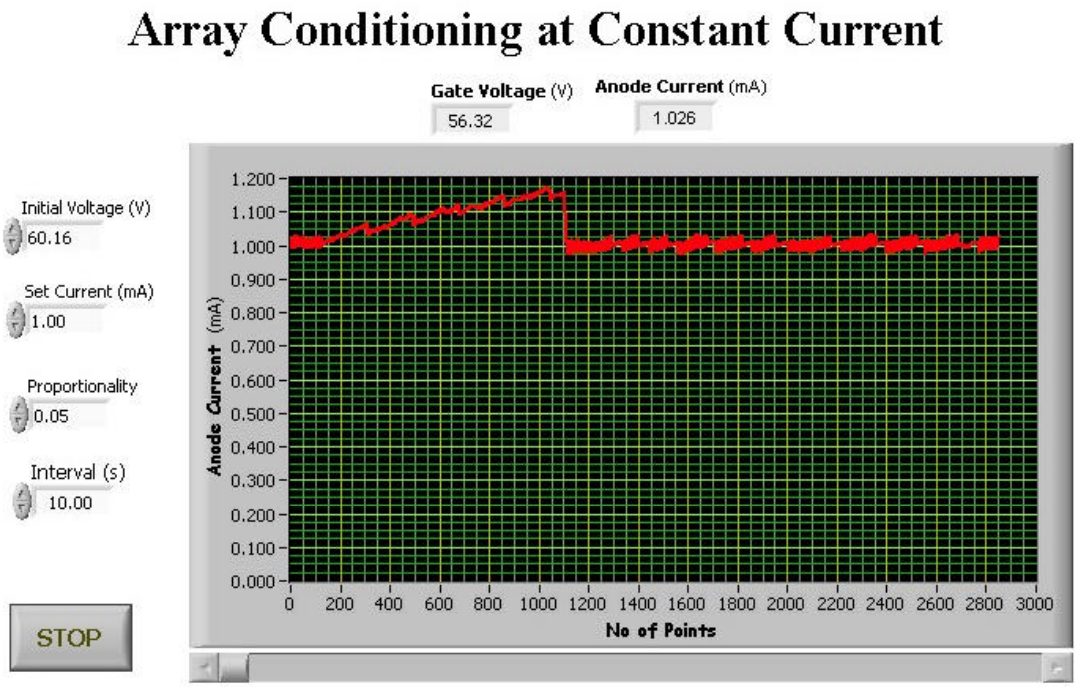

Figure 4.1 Screen view of a tip conditioning experiment done at constant current of 1mA. The initial gate voltage was 60V reducing to 56V after 2 days.

Tip conditioning is not done at a constant gate voltage because, as the tip gets cleaner, the work function reduces resulting in a large increase in emission current. For this reason, tip cleaning is done at constant current using a feedback controller, which automatically adjusts the gate voltage to get the set point value of emission current.

The initial gate voltage required to get 1mA was 60V and after 80000 s (1 day), the voltage dropped to 56V. The array was then switched off for 3 days and the above process was repeated for a higher current.

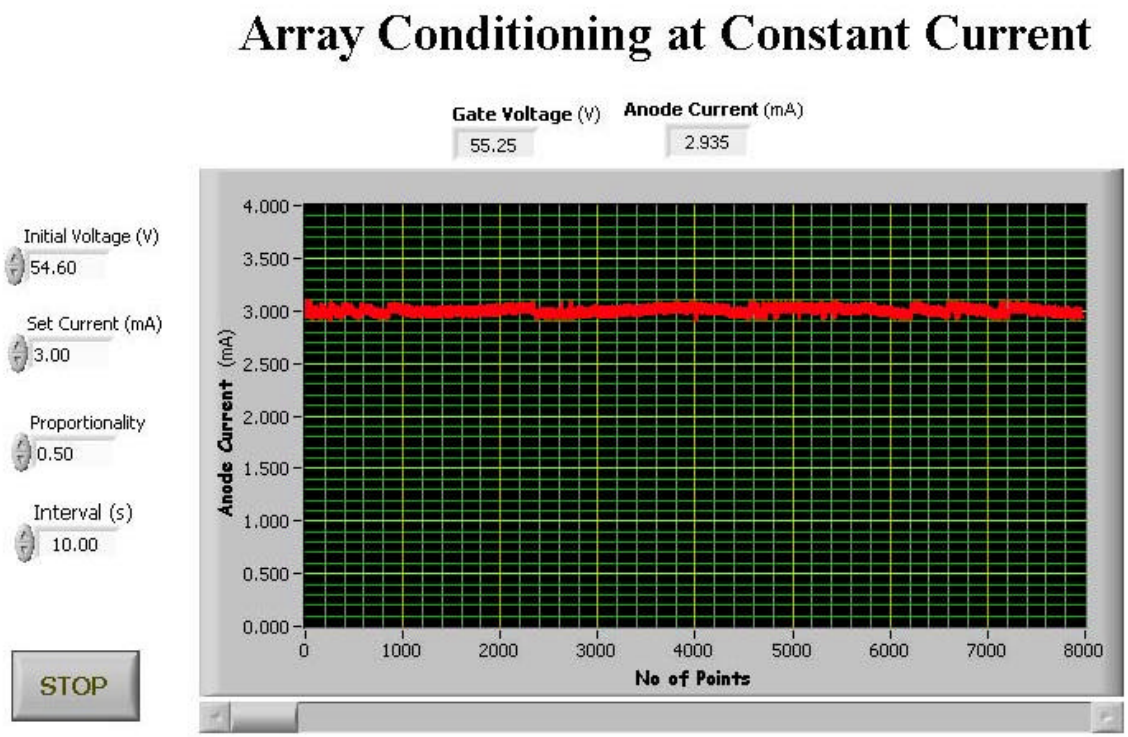

Figure 4.2 Tip conditioning for a stable FEA, being conditioned at 3 mA. Even after one day, the change in voltage was < 1V (i.e. the tip was quite stable).

The tip conditioning of a stable FEA, cleaned for 2 days is shown in Figure 4.2. In order to understand the effect of conditioning on the emission characteristics of the FEA, several I-V and F-N plots were recorded during the course of the experiment. The pressure of the UHV test chamber was 3.0×10^{-8} torr before switching on the array.

4.2.2 Tip Analysis (I-V and F-N data)

In order to measure the emission characteristics of the FEA, several I-V and F-N plots were acquired. The F-N plot provides an indication of the work function, tip geometry (slope of the FN plot) and average emission area (y – intercept of the FN plot) as seen in Figure 4.3.

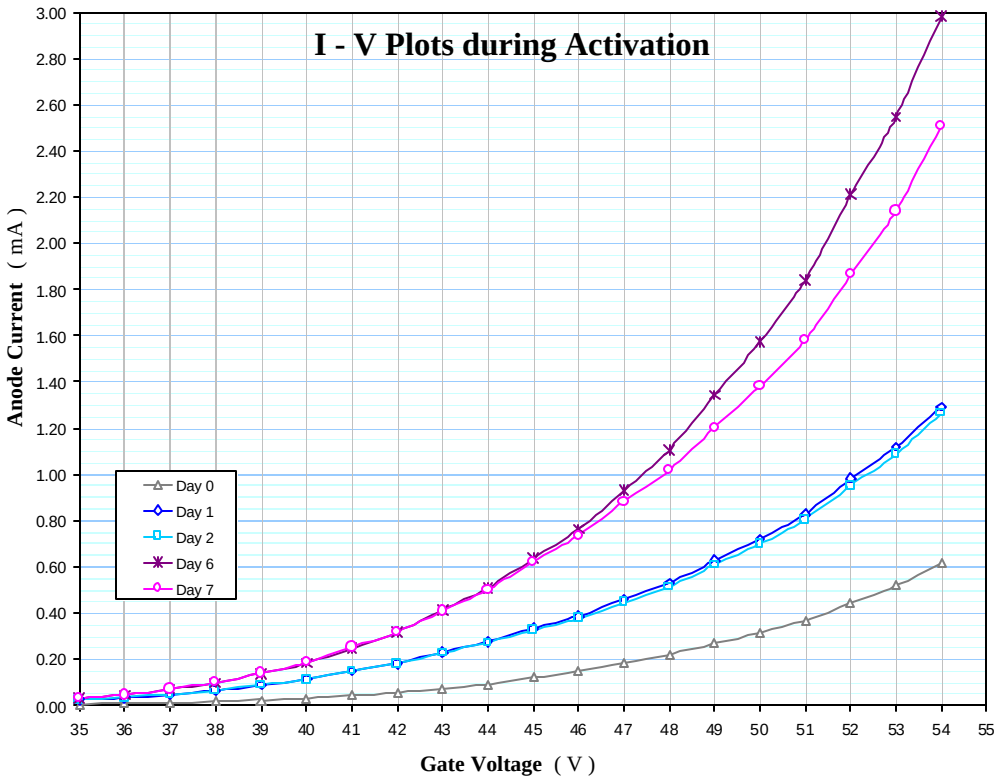

Figure 4.3 I-V plots taken before and after the FEA was conditioned. As we ran the FEA for longer periods of time, we see tip cleaning in the form of higher emission current for the same voltage.

To get an idea of the tip geometry, work function and emission area, F-N plots are shown in Figure 4.4. We ran the experiment for a week, starting on day 0 we took an I-V plot and then on day 1 (24hrs) and day 2 (48hrs). We switched off the FEA on day 3

(72hrs) for 3 days i.e. we switched on the FEA on day 6 (144hrs). Then we again conditioned the FEA from Day 6 (144hrs) to Day 7 (168hrs), after which we switched off the FEA. The above tip conditioning, was done at a constant current of 1mA. The initial gate voltage needed for 1mA was 60.16V. During the tip conditioning process, the gate voltage was reduced (as the tips got cleaner) and reached 56.32V after 48hrs of operation (day 2).

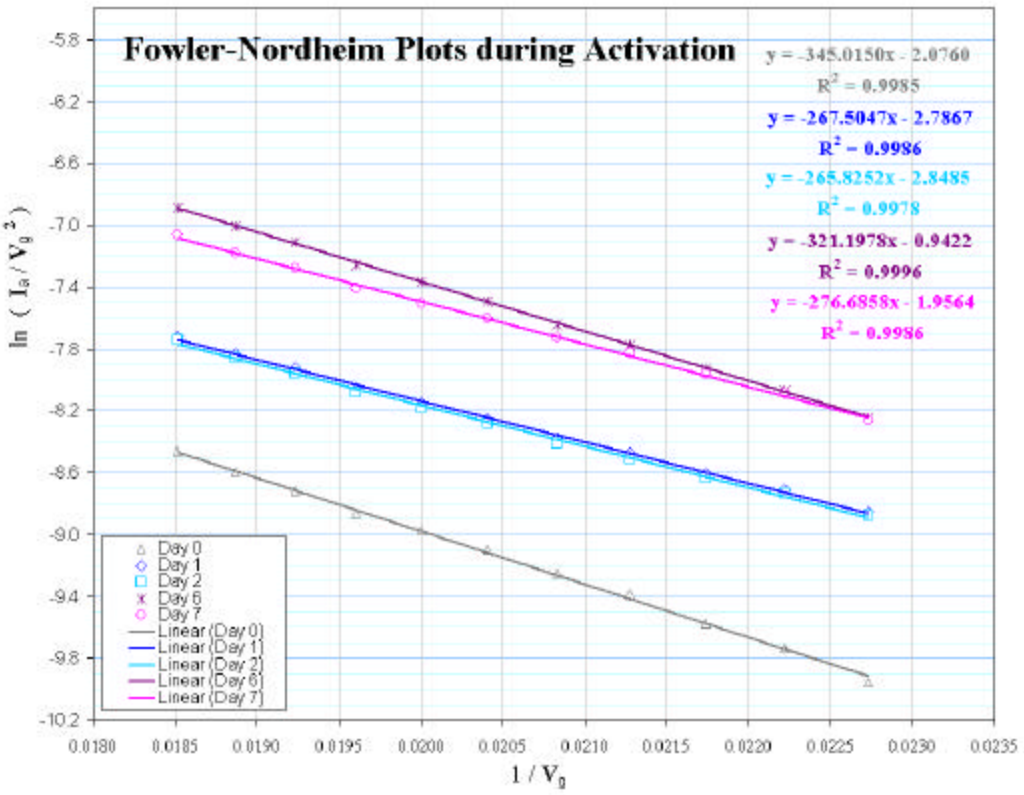

Figure 4.4 F-N plots taken before and after the FEA was tip conditioned. As we ran the FEA for longer periods of time, we see tip cleaning (reduction in slope and lowering of the emission area).

During tip conditioning, there is a reduction in slope and emission area (reduction in work function, due to cleaning since the tip geometry does not change for small O_2

exposures[1]). When we switch the FEA off, from the 3rd day till the 5th day, there is an increase in slope due to some tip oxidation, which is less than the starting value as the FEA was in UHV i.e. 3.0 $\times 10^{-8}$ torr. There was a considerable increase (almost 7 times) in emission area as indicated by the FN plot Y – intercept. This can be attributed to more tips emitting.

When we do another tip conditioning experiment from day 6 (144hrs) to day 7 (168hrs) and we see a reduction in the slope due to cleaning and a reduction in emission area (almost 3 times) which may be due to the reduction of the number of emitting tips.

4.3. DC Mode Degradation – Experimental

4.3.1 Degradation as a function of Gate Voltage

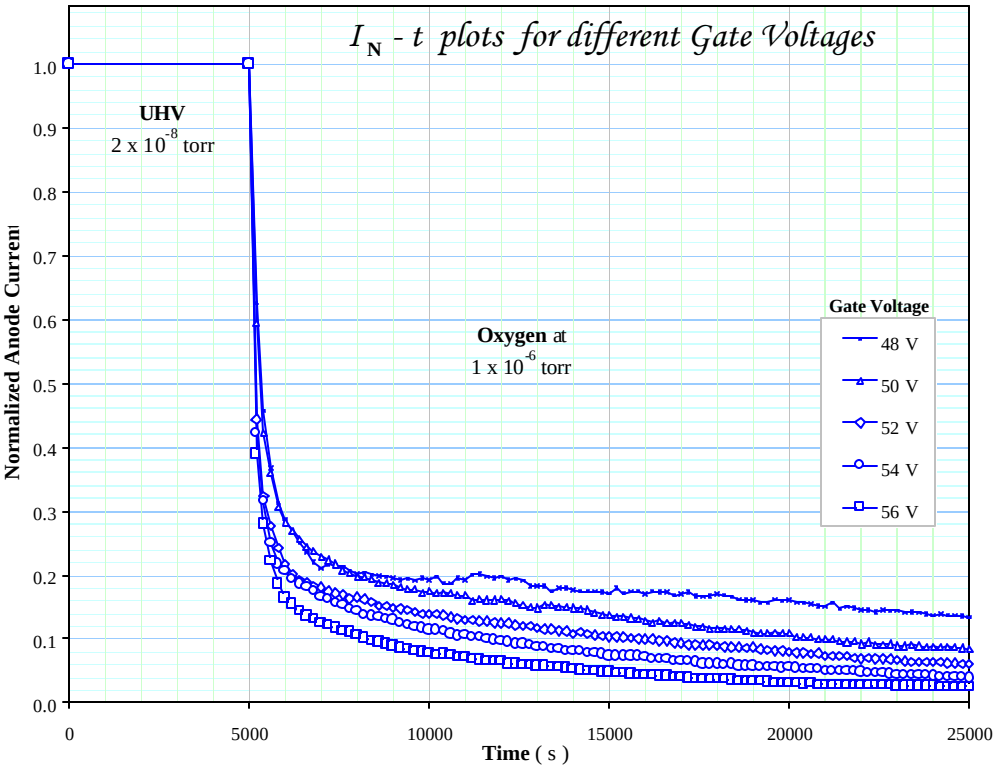

Figure 4.5 I_N - t degradation as a function of initial gate voltage in DC Mode

The DC mode degradation experiments were done for different initial gate voltages (48V, 50V, 52V, 54V and 56V). This was done to determine whether the arrays could be stable in O_2 if they were run at lower voltages. The FEA was first tested for emission current stability for 5000s (to have less than a 0.5% change) before exposing it to O_2. After the degradation experiment, the O_2 was pumped out and the gate voltage was increased to a higher value (slightly higher than the gate voltage required for the next experiment).

In view of the coupled nature of these interactions, it is not possible to separate the effects due to the high electric field and the field emitted electron density. The degradation in emission current after 20000L O_2 exposure was measured for different gate voltages (48, 50, 52, 54 and 56V) and is presented in Figure 4.5. The initial anode currents were not the same and varied from 0.6mA to 3.3mA.

The degradation as a function of exposure follows an exponential behavior at low exposure doses until 5000L after which it follows a linear relation. The extent of degradation increases as a function of gate voltage, from 86% at 48V to 97% at 56V, which is almost a 11% increase in degradation.

4.3.2 Changes in Slope & y - intercept

In order to relate the emission characteristics to the surface properties, the changes in slope and y - intercept, after every exposure were measured. Changes in work function or tip geometry are reflected in the slope of the F-N plot and the changes in area are reflected in the y - intercept.

In the field emitter arrays tested, a layer of amorphous Si is placed below the Mo emitters as seen in Figure 4.6, for current limiting, and thereby preventing catastrophic

failures. The resistance of the amorphous Si layer affects the emission current. Therefore, to accurately calculate the changes in work function, the voltage drop across the amorphous Si layer has to be taken into account.

Various models for estimating the resistance for such arrays have been proposed[3,4], but it was found that by fitting the data in a low emission current regime, the perturbation induced by the resistive layer on the slope can be avoided and we can get good estimates of the value of the F-N curve.

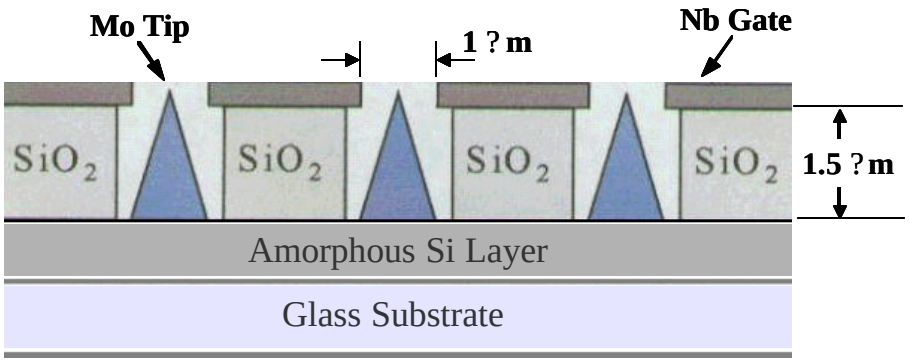

Figure 4.6 Schematic of a typical Spindt-type Mo Field Emitter Array[5]

As we go to higher voltages, the emission current starts to turn over. This is due to current limiting effect of the amorphous Silicon layer as shown in figure 4.7, which also helps in maintaining current uniformity from the tips, and thus preventing catastrophic failures due to high emission current from the emitting tips.

Since the FEA was exposed to 20000 L of O_2, the change in the slope of the F-N plot after each degradation experiment was significant. There is also a significant change in the tip geometry, apart from the change in work function and emission area as shown in Table 4.1.

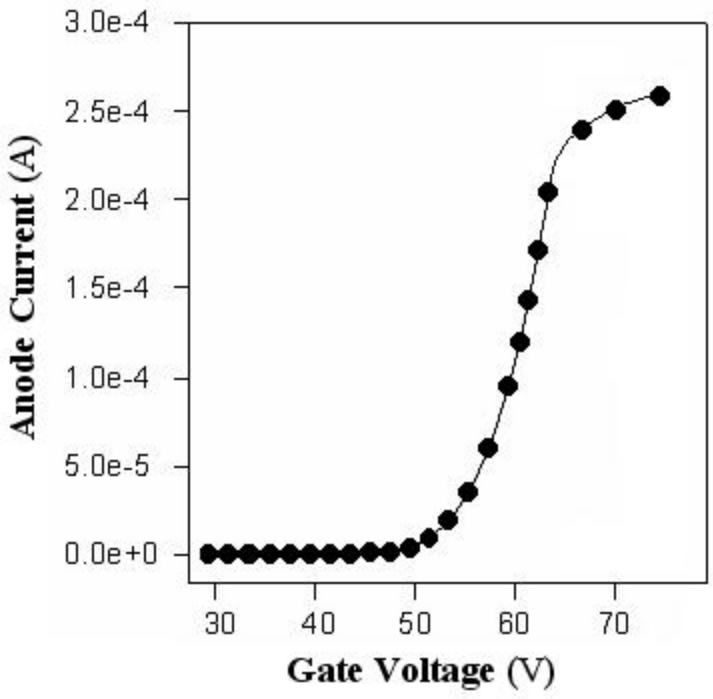

Figure 4.7 I-V Curve for higher voltages. At higher voltages, due to the amorphous Si layer, there is a current limiting effect.

Day	V_g (V)	F-N Slope		F-N Y- intercept		% Change in Slope	% Change in Area
		Before	After	Before	After		
1	48	-420.1	-608.6	0.6	2.5	44.9%	568.6%
2	50	-419.1	-627.6	1.0	2.4	49.7%	305.5%
3	52	-418.1	-664.2	2.0	2.5	58.9%	64.9%
4	54	-417.1	-678.2	2.0	1.9	62.6%	-9.5%
5	56	-456.3	-659.4	2.2	1.2	44.5%	-63.2%

Table 4.1 Change in the F-N Slope and y - intercept after O_2 degradation experiments for different Gate Voltages.

The change in F-N Slope after the O_2 exposure, assuming all the Mo forms MoO_2, would be 41.6% (from 4.6eV to 5.8eV). From our results we see a higher % change, which indicates that apart from the change in work function due to oxidation, there is also a change in tip geometry.

4.4. Estimating the Life of the FEA

To get an idea of the lifetime of the FEA, we do a linear fit from 22000s to 25000s of degradation time (since the I-t plot is linear) as shown in figure 4.8. The mean lifetime ? is the solution extrapolating the straight line to zero emission current.

Each time we did a degradation experiment for 20000 L (20000s at 1.0×10^{-6} torr), there was a reduction in the estimated value of the lifetime. The reduction in lifetime after each experiment was not a constant and varied from 2000s to 11000s. The possible explanation was that as we did more experiments on the same FEA, there was some permanent change in tip geometry as seen in table 4.1.

Expt. No.	$\mathbf{V_g}$ (V)	$\mathbf{I_a}$ (mA)	**Life** (s)
1	48	0.659	57524
2	50	0.944	55596
3	52	1.398	44373
4	54	1.689	38621
5	56	3.333	31410

Table 4.2 Summary of the mean lifetimes of the FEA for the given set of 5 degradation experiments for different initial gate voltages.

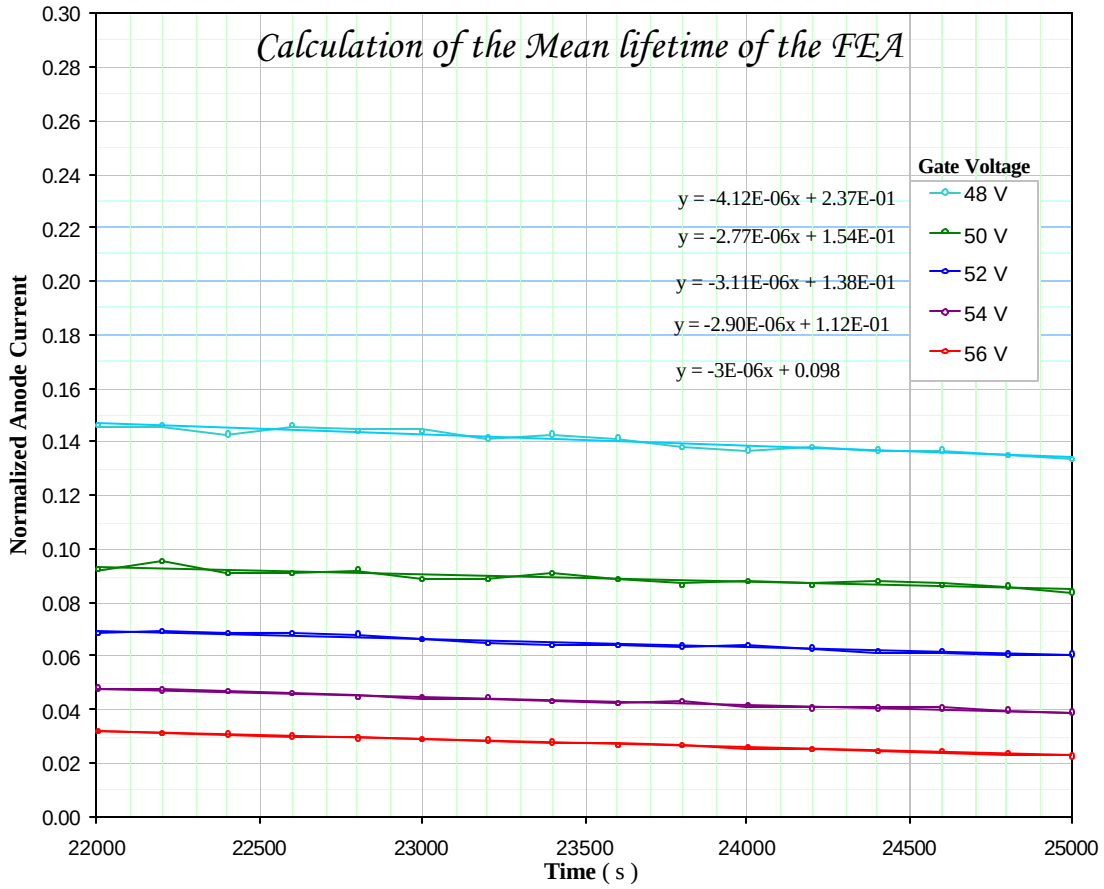

Figure 4.8 Mean lifetime estimation for the FEA for degradation experiments done at different gate voltages.

4.5. Pulsed Mode Degradation – Experimental

Measuring the degradation in dc mode results in 200x acceleration in device lifetime testing (assuming a 0.5% duty cycle for normal operation), provided emission degradation depends only on total exposures and not on duty cycle. Degradation measurements were made in the pulsed mode at 100 Hz with “ON duty Cycles” of 0.5%, 1.0%, and 5% compared to the dc mode of operation (100%).

"ON duty cycle" is defined as the fraction of time the device is on to the total operation time (ON time + OFF time). In our experiments, the exposure dose, is the "nominal exposure dose" which is not the same as "true exposure dose" as shown below:

A) Nominal Exposure Dose (L) : It is simply the area of the P-t curve when pressure is expressed in ??$^{????}$?torr and time in s. It does not take into account the % duty cycle, so a 20000L degradation experiment, done at 0.5% duty cycle and at 100% duty cycle would have the same nominal exposure dose of 20000L.

B) True Exposure Dose (L) : It is the product of the nominal exposure dose and fraction of the ON duty Cycle. A 20000L degradation experiment, done at 0.5% duty cycle would have a true Exposure dose of only 100L.

4.5.1 Degradation as a function of initial Anode Current

The pulsed mode degradation experiments were done for initial anode currents of 23mA, 31mA and 40mA. The gate voltages corresponding to these currents were 55V, 59V and 64V. The "ON" duty cycle was set to 0.5%, with an "ON" time of 50ms and an "OFF" time of 9.95ms. The FEA was conditioned for 3 days until there was stability in emission current. Before each degradation experiment, the FEA was run for 5000s to check for stability (<0.5% change in emission current).

The I-t degradation graph is shown in figure 4.9. There was very little difference in the extent of degradation for the above anode current values since the extent of degradation is strongly dependent on the initial gate voltage rather than the initial anode current. For 23mA, there was about 72% degradation, for 31 and 40mA there was about 77% degradation in emission current. To get an idea of the extent of degradation in the pulsed mode and DC mode, both I_N-t graphs have been superimposed (figure 4.10).

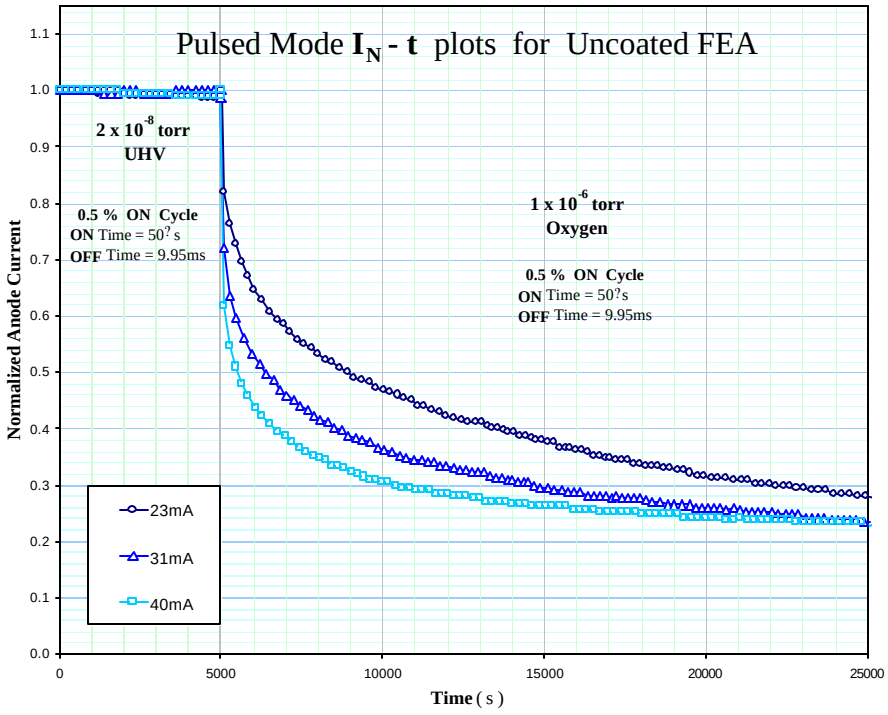

Figure 4.9 Pulsed mode I_N – t degradation at 0.5% duty cycle for different anode currents.

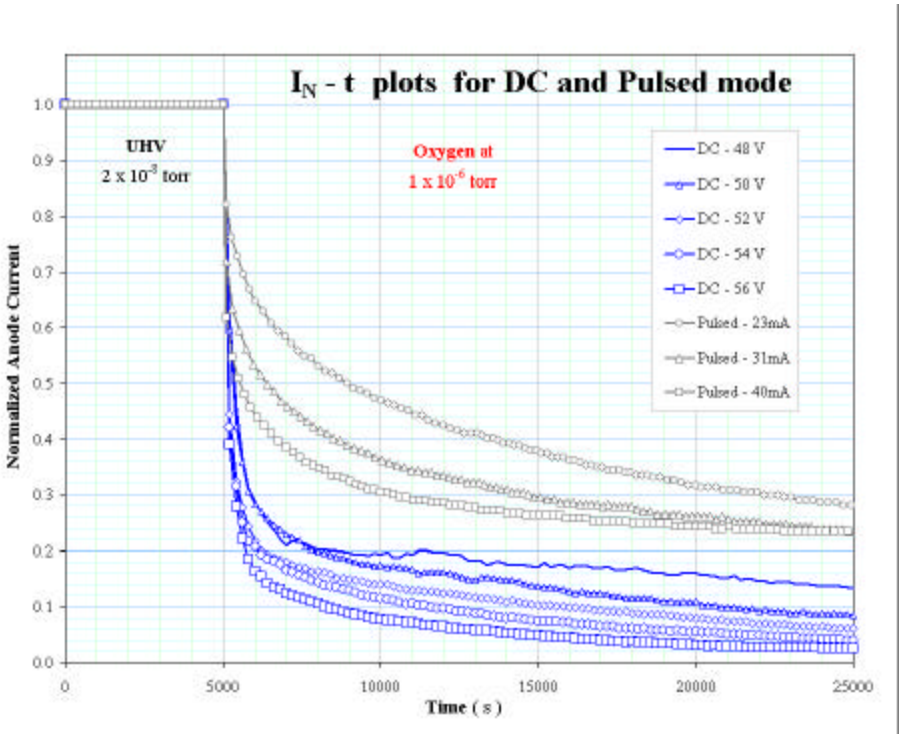

Figure 4.10 I_N – t plots for the O_2 degradation experiments in DC mode and pulsed mode at 0.5% duty cycle.

4.5.2 Anode Current Recovery

After each of the above degradation experiments, the O_2 was pumped out from the UHV chamber and the duty cycle was increased to 25% at the same voltage. The time of recovery to 100% emission current took over 10 hours after which it was stabilized at constant anode current for several hours.

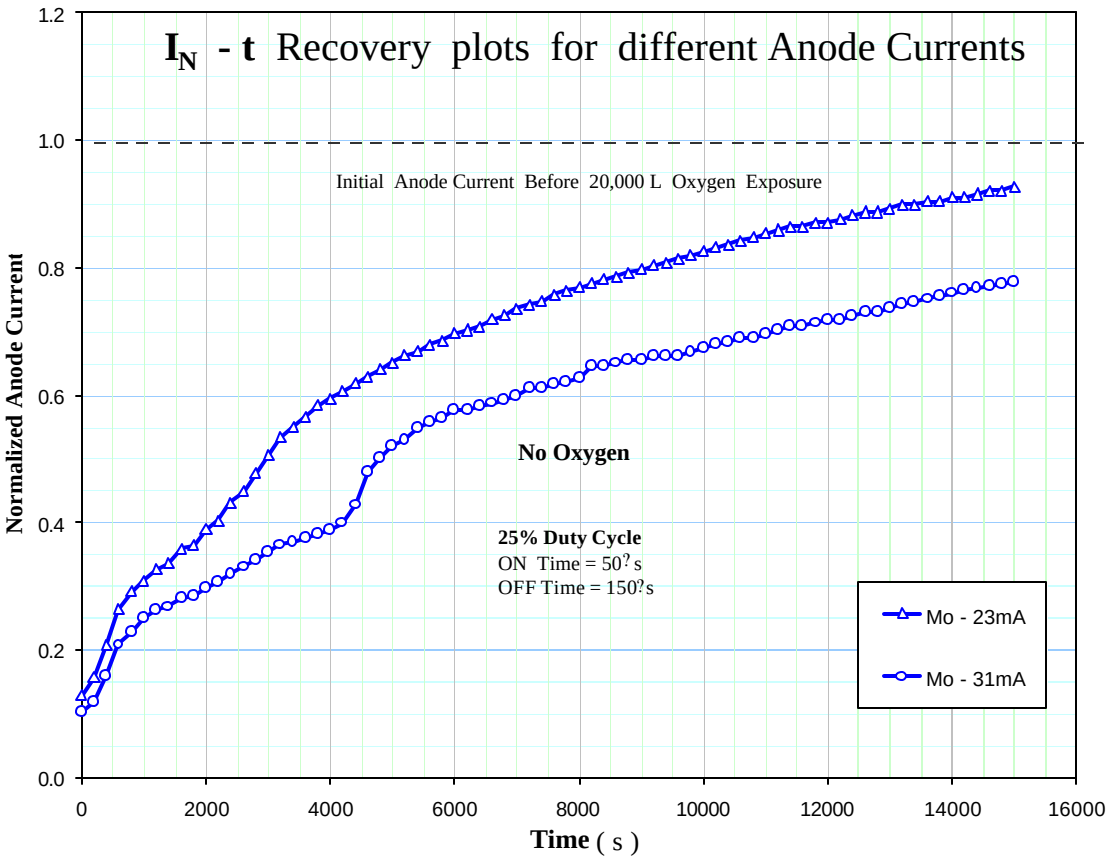

Figure 4.11 Graph showing normalized anode current recovery after the O_2 was pumped out of the UHV chamber.

4.6. Results and Discussion

All the Mo FEAs have shown significant degradation in emission current when exposed to O_2. Their I-V emission characteristics were measured before and after the O_2

degradation experiments. For the degradation experiments done in DC mode and later in the Pulsed mode, we observed that the extent of degradation was higher in DC mode than the pulsed mode experiments at 0.5% duty cycles, which indicated that oxidation occurred even when the device was “OFF”.

REFERENCES

[1] B.R. Chalamala, R.M. Wallace, B.E. Gnade, J. Vac. Sci. Technol. **B16**, 2859 (1998).
[2] Labview 6.0i, National Instruments Inc., Austin, Texas (2000).
[3] J.D. Levine, R. Meyer, R. Baptist, T.E. Felter and A.A. Talin, J. Vac. Sci. Technol. **B13**, 474, (1995).
[4] J.D. Levine, J. Vac. Sci. Technol. **B13**, 553 (1995).
[5] B.R. Chalamala, Thesis (PhD.), University of North Texas 1996.

CHAPTER 5

STABILITY OF GOLD COATED FIELD EMITTER ARRAYS

5.1. Introduction

For a good field emission material, apart from having a low work function, it should be mechanically stable, easy to fabricate and should not be oxidized easily. Enhancements in field emission from Si tips, covered by super thin diamond-like carbon films were investigated by Litovchenko *et. al*,[1] who also studied the effect of different types of coatings and surface treatments (electrochemical etching, H^+- implantation, and Cs enriched layers) on the electron field emission from Si tips. Coatings of Cu-Li alloy films on gated Si tips, resulted in a very low emission voltage.[2]

Several Ir field emitter arrays were fabricated by Chalamala *et. al*, who reported that in spite of a slightly lower aspect ratio compared to Mo, in the presence of O_2, Ir FEAs showed improved current stability to their Mo counterparts.[3] The pressure dependency of emission currents of Si, Mo, Au and SiC field emitters were investigated and also showed improved emission current stability.[4]

The effect of in situ carbon coatings on spindt type Mo tips was investigated by Mousa *et. al*, who reported an increase in stability of field emission current after the coating process.[5] The emission stability of Mo FEAs coated with diamond-like carbon films, was investigated.[6] Field emission from diamond coated field emitters yielded significant increase in emission current and lowered the F-N slopes.[7] By applying a thin layer of Cesium on FEAs, there was a significant reduction in operating voltage.[8] Similar effects were observed by depositing K and Li on Spindt type microcathode arrays.[9]

Electron emission enhancement by coating Spindt type field emitter array cathodes with several monolayers of Ti, Zr and Hf has also been reported.[10] Nitrides of transition metals like Nb, Zr and Ti were fabricated and tested for emission current stability.[11] Coating Mo FEAs with thin ZrC films resulted in almost a ten-fold increase in the emission current level.[12]

In this chapter, we present the results of the experimental measurements on the interaction of O_2 with Au coated Mo FEAs. The stability of the FEA to O_2 exposure was found by measuring the emission and device recovery characteristics as a function of total O_2 exposure. The device lifetime resulting from O_2 exposures for longer periods of time is determined and the results are discussed.

Au does not oxidize easily and thus the change in work function due to O_2 exposure should be very small. Emission current degradation is sensitive to the fraction of the area of the uncoated FEA (Mo). The O_2 degradation tests have been carried out for different initial gate voltages, anode currents and duty cycles. The uniqueness of this kind of lifetime testing is that the Au coated half of the array and the uncoated half are subjected to identical conditions of O_2 exposure.

5.2. Au Coated Field Emitter Arrays - Experimental

Experiments were performed with six Au coated Spindt-type field emitter arrays. The arrays were manufactured by Pixtech for Texas Instruments. Of these, two FEAs were coated with Au on one half of the emission area, while the other half was uncoated. The first FEA was coated with 29Å of Au on one half of the emission area, while the other half was uncoated. All experiments were done in the pulsed mode for different duty cycles (0.5%, 1% and 5%) and the anode voltage was set to 320 V.

Most experiments were carried out in pulsed mode at 0.5% duty cycle, with an ON time of 50?s and an OFF time of 9.950ms. Using a dual 300MHz oscilloscope, we were able to measure the voltage drop across a 330? Resistor connected to the circuit. Dividing the voltage drop by the resistance we were able to calculate the anode current for the Au coated and the uncoated half. The delay between measuring the emission current from the uncoated and the Au coated side when ON, was 5ms.

A second FEA was coated with 25Å of Au on one half of the emission area, while the other half was uncoated. Similar experiments were performed on this array, but the measurements were only made for the Au coated half. The last four arrays were coated with 22Å, 45Å, 66Å & 90Å Au respectively. Using accelerated tests at 5% duty cycle, the long-term stability to O_2 exposures was measured. For anode current recovery, the duty cycle was increased to 25% without changing the gate voltage.

5.3 Emission Characteristics

5.3.1 Current-Voltage & Fowler-Nordheim Data

The array was activated at 3mA for two days before any tests were carried out. The I-V plot (Figure 5.1) is shown along with the Fowler-Nordheim plot of the 29Å Au coated half of the FEA along with the uncoated half (Figure 5.2). It was observed that the emission area of the Au coated half was much less than that for the uncoated half.

This strongly indicated that only a small fraction of the Au coated tips were actually emitting. Also, the anode current from the Au coated half for the same gate voltage, was almost an order of magnitude less than that for the uncoated (Mo) half. This was mainly due to the higher work function of Au.

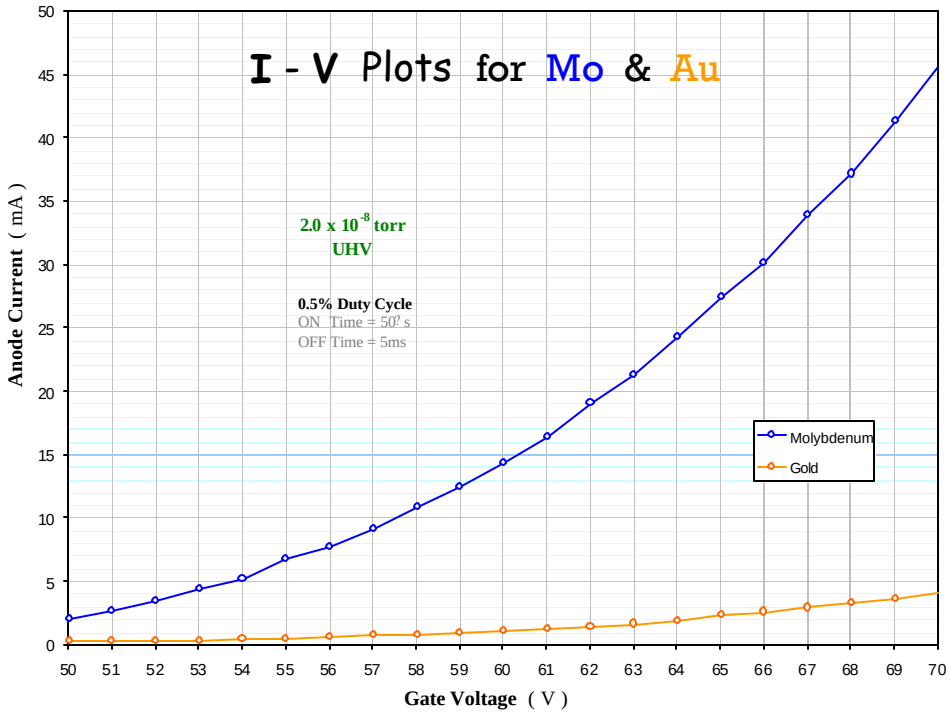

Figure 5.1 I-V curves, for the Au coated half and the uncoated Mo half.

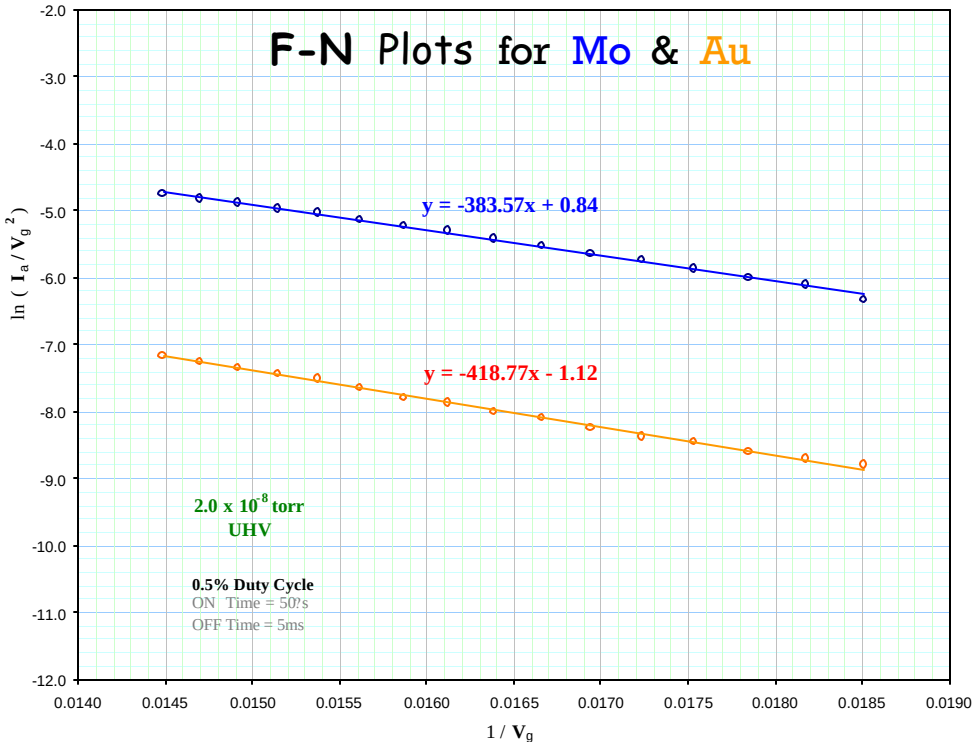

Figure 5.2 F-N plots, for the Au coated half and the uncoated Mo half.

Applying the Fowler-Nordheim equation, we can estimate the ratio of the emission areas of the uncoated side to that of the coated side. Using the work function values of Au and Mo, and from the slope of the F-N plot, the change in the field enhancement factor (tip geometry) after Au deposition, was calculated.

From the FN plots in Figure 5.2, the slopes for the Au coated half and uncoated (Mo) half are seen to scale with their work function. Using the values of the work function for Au and Mo, and from the FN slopes we can determine the ratio of the field enhancement factor (b_{Au} / b_{Mo}) before and after the Au deposition, using equation (5.1) :

$$(b_{Au} / b_{Mo}) = (?_{Au} / ?_{Mo})^{-3/2} (m_{Au} / m_{Mo}) \qquad (5.1)$$

where, $?_{Au}$ and $?_{Mo}$ are the work functions of Au and Mo, and m_{Au} and m_{Mo} are the FN slopes for the Au coated half and uncoated half (Mo).

Using the work function values for Au and Mo and from the above slopes , we get

$$(b_{Au} / b_{Mo}) = 0.83 \qquad (5.2)$$

and the ratio of emission areas (A_{Au} / A_{Mo}) = 0.14 which indicates that only a fraction of tips are emitting from the Au coated half.

5.3.2 Degradation as a function of the Gate Voltage

The O_2 degradation experiments were done for 2 gate voltages i.e. 65V and 70V for a dose on 20000L. The initial anode currents from the Au coated half and uncoated half, were different for the same gate voltage. The current versus dose plot for 65V and 70V, are shown in Figure 5.3.

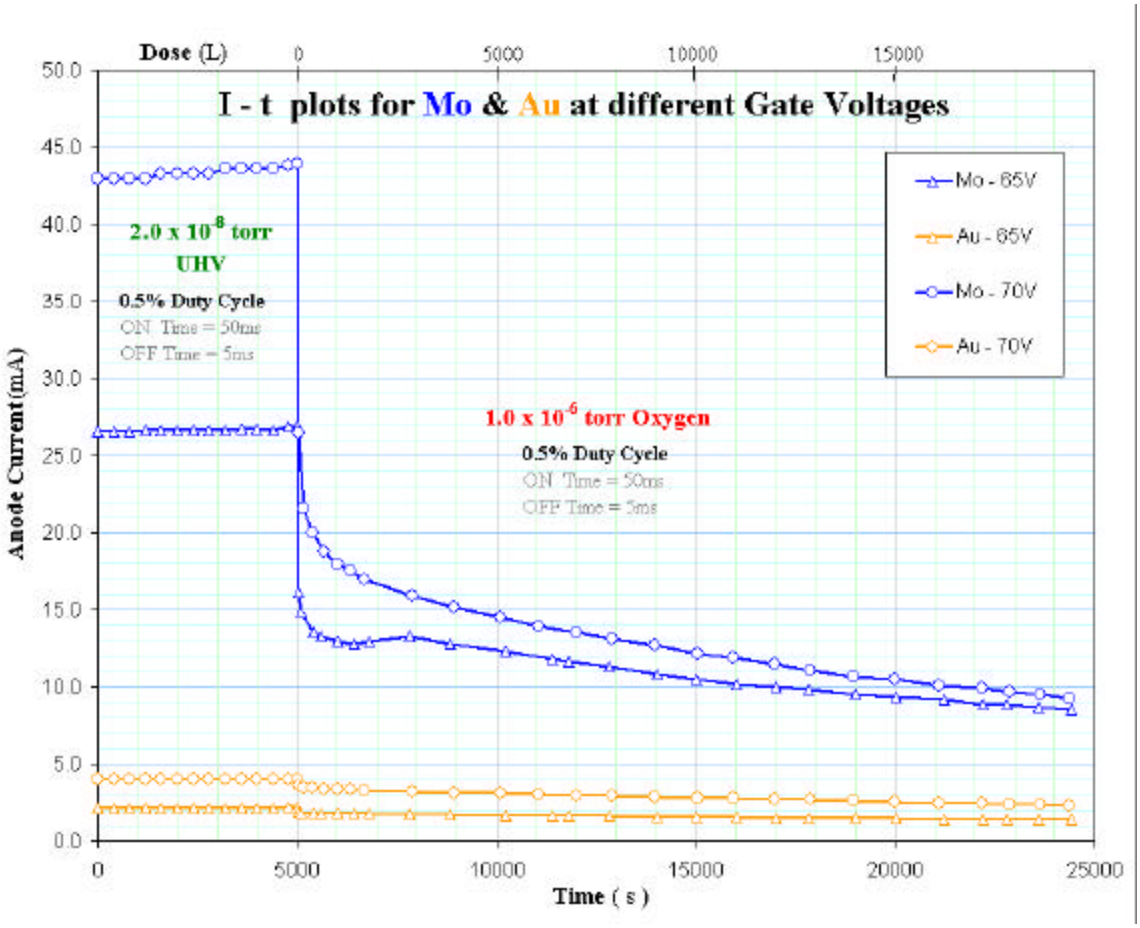

Figure 5.3 I-t degradation for different gate voltages, for the Au coated half and the uncoated Mo half.

The normalized current versus dose plots, are shown in Figure 5.4. For the uncoated side, increasing the gate voltage increases the extent of degradation but for the Au coated side the change was not so significant.

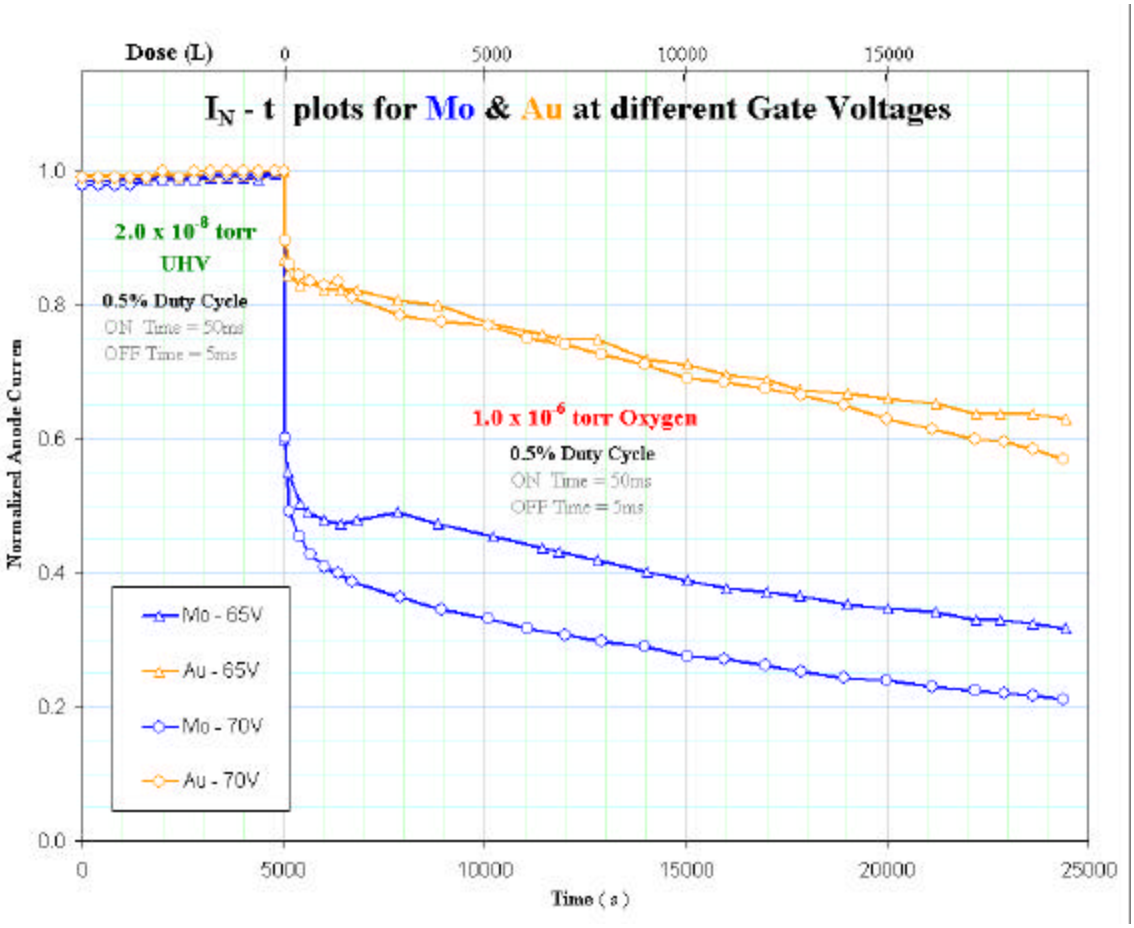

Figure 5.4 I_N-t degradation for different gate voltages, for the Au coated half and the uncoated Mo half.

5.3.3 Degradation as a function of the initial Anode Current

The O_2 degradation experiments were done for 5 different anode currents i.e. 15mA, 28mA, 35mA, 41mA & 53mA as shown in Figure 5.5. The gate voltage for the Au coated half was approximately 15 – 20V higher than that for the uncoated (Mo) half in order to have the same current on the Au coated and uncoated (Mo) half.

At first the array was tested for stability i.e. the anode current should have less

than 5% change after running for 5000s. The system had a base pressure of 2×10^{-8} torr before O_2 was introduced. Then 1×10^{-6} torr O_2 was gradually introduced into the chamber through a leak valve. Each of the above experiments ran for over 6 hrs.

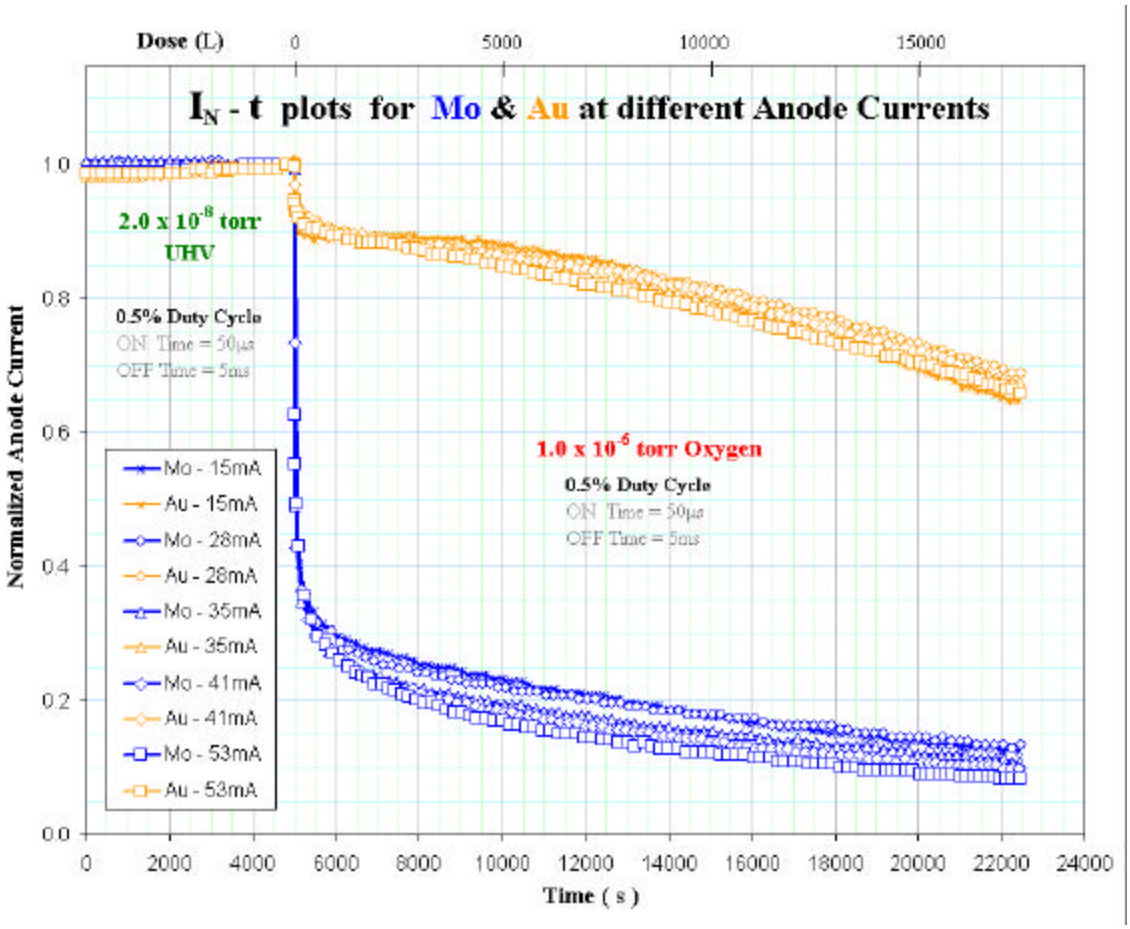

Figure 5.5 I_N-t degradation for different anode currents, for the Au coated half and the uncoated Mo half.

5.3.4 Recovery of Anode Current

When the degradation was complete, the O_2 in the chamber was pumped out and the duty cycle was increased to 25%. The anode current was allowed to recover for a few hours until it attained its starting value. For the Au coated side, the recovery was quick

(15min) and the final current exceeded its initial value. This indicates that there may have been some MoO_2 on the FEA tips before they were coated with Au. After each degradation experiment, the FEA was cleaned by increasing the duty cycle. The process of oxide removal, was indicated by a reduction in the work function.

After emission current recovery, the gate voltage was further increased. The duty cycle was then changed to 0.5% and the system was allowed to run for several hours until the anode current was stabilized (less than 0.5% change in emission current). The results of the emission current recovery are shown in Figure 5.6 below.

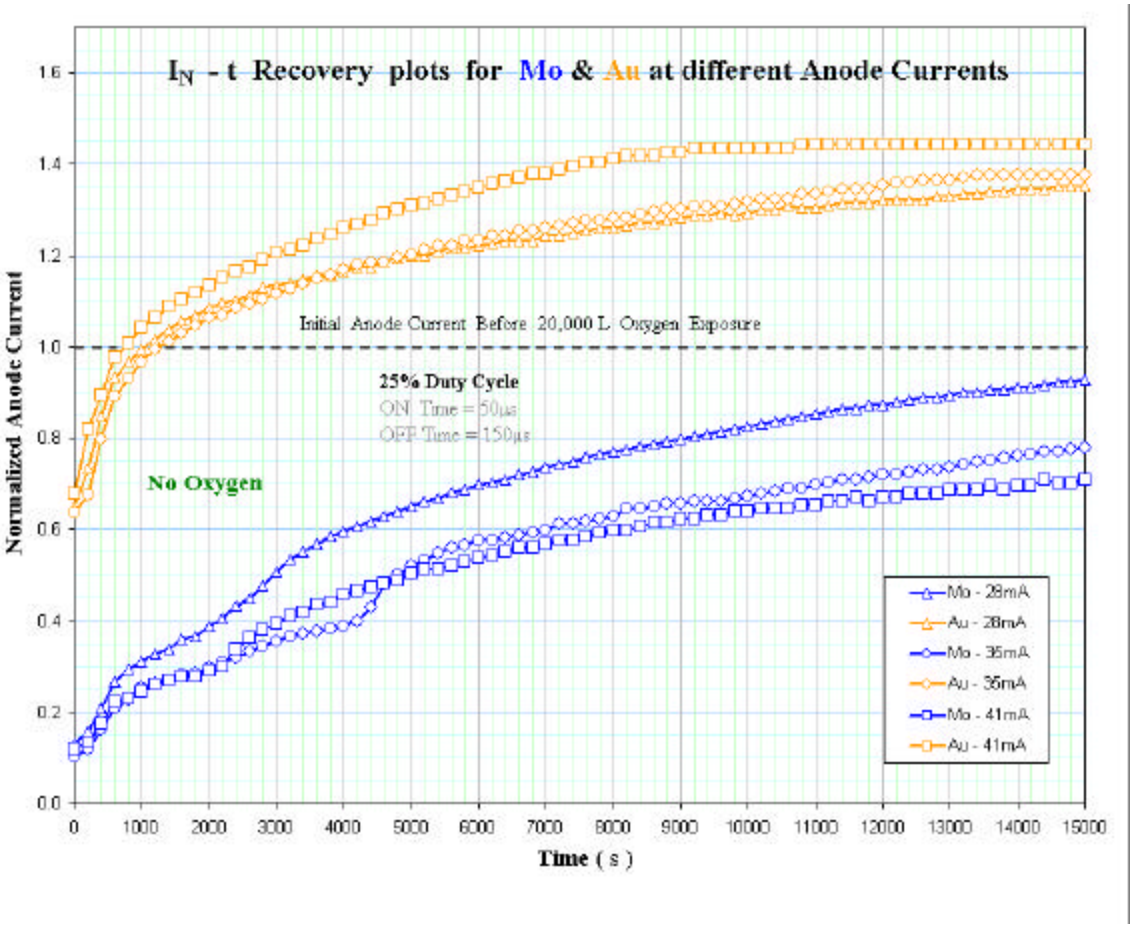

Figure 5.6 I_N-t recovery plots for different anode currents, for the Au coated half and the uncoated Mo half.

5.3.5 Degradation as a function of the Au thickness

The accelerated tests at 5% duty cycle were performed for a long period of time (200,000s). The overall dose was 100 times larger than the earlier 20000s degradation tests. For this set of experiments, the arrays were completely coated with Au films of thicknesses of 22 Å, 45 Å, 66 Å and 90Å. An uncoated array was used as the control sample. The initial anode current for each of the above arrays was approximately 53mA, after activating each array for 2 days and stabilizing for 20,000s. The summary of the degradation versus Au thickness is shown in Figure 5.7.

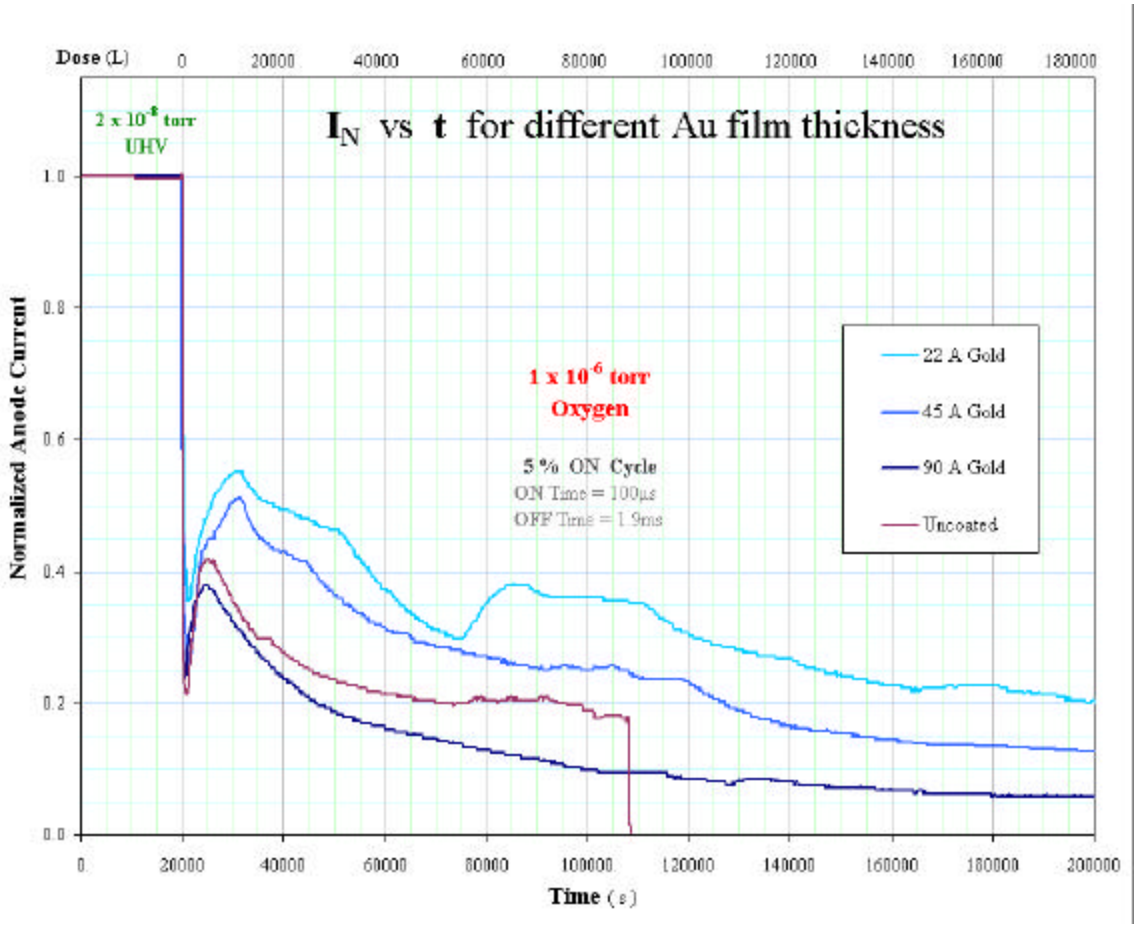

Figure 5.7 I_N-t degradation experiments for Au coated FEAs (long term stability at 5% duty cycle for 200000s)

5.4. Results and Discussion

For the arrays coated with 29Å and 25 Å Au on half their area, for the same applied gate voltage, we would get a much lower value of emission current from the Au coated side than from the uncoated side. This was mainly because of the higher work function of Au (5.5eV) as compared to Mo (4.6eV).

Also, not all the tips were emitting from the Au coated portion, which was indicated by a much lower area, compared to the uncoated portion. From the experimental data for the degradation at different anode currents for the above FEA, the Au coated side was seen to degrade much less (33%) than the uncoated side (90%) after 20000 L of O_2 exposure. Ideally, we would not expect any degradation in emission current from the Au coated half.

One reason for this degradation may be that not all the tips that are emitting, are coated with Au and there may be a small fraction of uncoated tips. The following is a method of estimating the fraction of Mo emitter tips in the Au coated half of the array.

The assumptions are that the anode current from the Au coated side does not change due to the Au coated tip degradation, the fraction of Mo remains the same throughout the experiment along with the tip geometry, as we recover the entire initial anode current.

Let f be the fraction of Mo tips and I'_{Au} be the current from only the Au coated tips.

For a 65V Gate Voltage,

Before Degradation: $I_{Mo} = 26.52mA$, $I_{Au} = 2.16mA$

After Degradation: $I_{Mo} = 8.56mA$, $I_{Au} = 1.37mA$

Thus the 2 equations, we have are :

$$2.16 = I'_{Au} \times (1 - f) + 26.52 \times (f) \quad (5.3)$$

$$1.37 = I'_{Au} \times (1 - f) + 8.56 \times (f) \quad (5.4)$$

Solving the above equations, we get f = **0.044** or **4.4**% uncoated Mo tips on the Au coated side.

For a 70V Gate Voltage,

Before Degradation: I_{Mo} = 42.94mA, I_{Au} = 4.00mA

After Degradation: I_{Mo} = 9.28mA, I_{Au} = 2.30mA

Thus the 2 equations, we have are :

$$4.00 = I'_{Au} \times (1 - f) + 42.94 \times (f) \quad (5.5)$$

$$2.30 = I'_{Au} \times (1 - f) + 9.28 \times (f) \quad (5.6)$$

Solving the above equations, we get f = **0.05** or **5.0**% uncoated Mo tips on the Au coated side.

From the above results, we see that, there is only a slight change in the fraction of uncoated tips. Also there is some sputtering of the Au coated tips and the fraction of uncoated Mo tips would thus increase as we do more degradation experiments. A 5% fraction of uncoated Mo tips in the Au coated half causes a significant degradation (33%) in emission current. The stability of the Au coated arrays is thus sensitive to the fraction of uncoated Mo tips. For a given Gate Voltage, we have the following :

$$D_{Au} = D_{Mo} \times f \times (I_{Mo} / I_{Au}) \quad (5.7)$$

Where,

D_{Mo} = % degradation of the uncoated (Mo) portion

D_{Au} = Apparent % degradation of the Au coated portion

f = Fraction of Mo in the Au coated portion

I_{Mo} = Anode current from the uncoated (Mo) portion

I_{Au} = Anode current from the Au coated portion

The above equation works well for an Au coated array with a very small fraction of Mo (Since I_{Au} I'_{Au})

The long-term stability tests were done for 4 Au coated arrays of thickness 22 Å, 45 Å, 66 Å and 90Å The results showed more or less the same amount of degradation for the Au coated FEAs and the uncoated FEA. The main reason for this was that the FEAs may have not been coated with Au completely and this was strongly indicated from their I-V data shown in Figure 5.8 and F-N data shown in Figure 5.9.

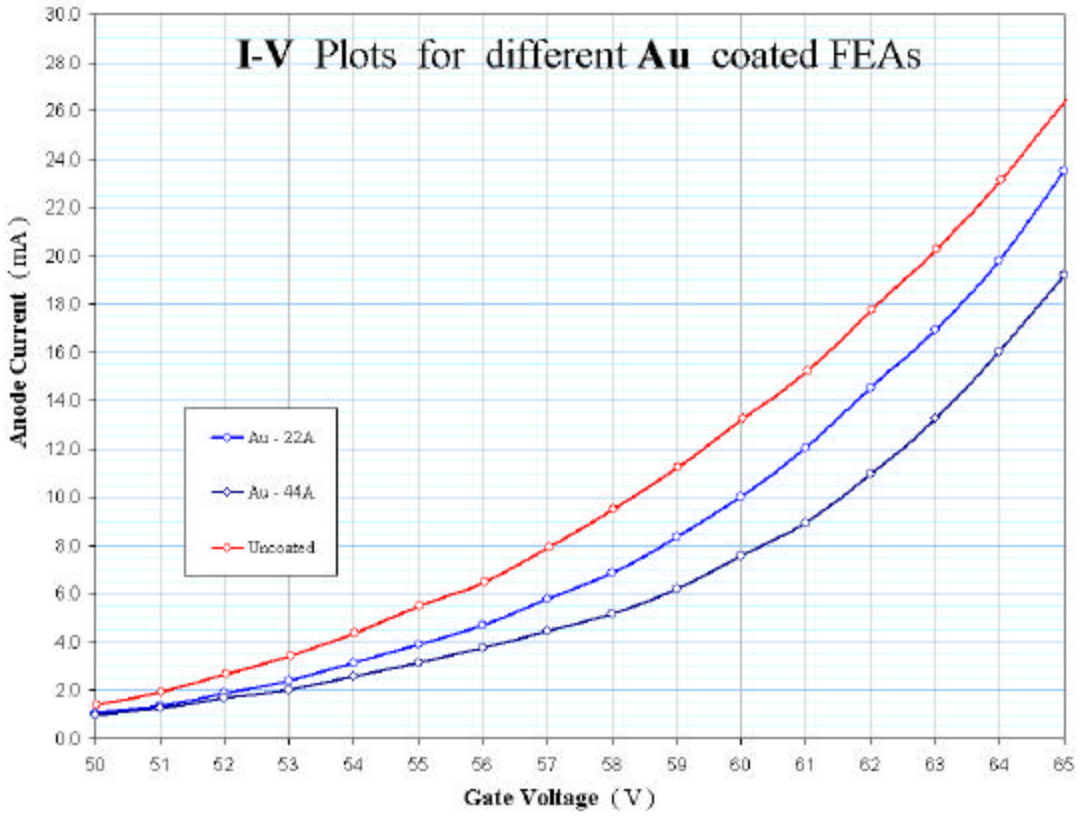

Figure 5.8 I-V curves for 2 Au coated FEAs and an uncoated FEA showing similar emission characteristics.

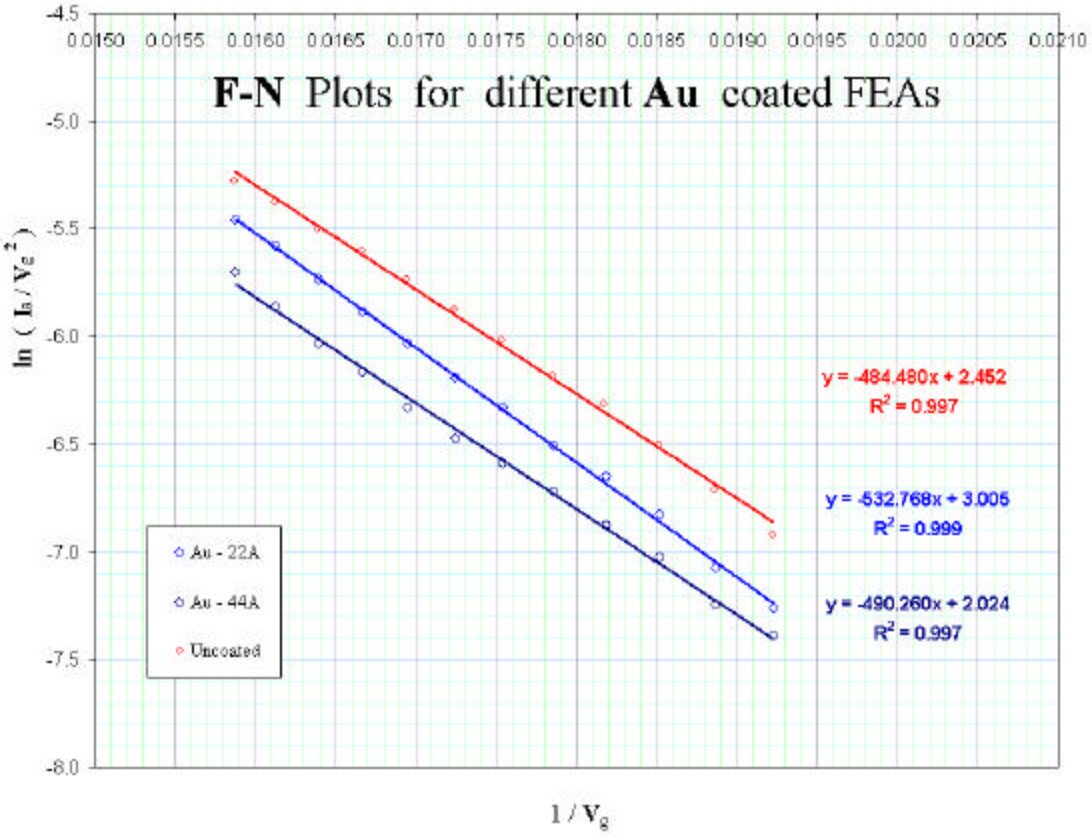

Figure 5.9 F-N plots for 2 Au coated FEAs and an uncoated FEA indicating similar emission characteristics.

For the FEAs coated with Au only on one half of their area, for a given emission current, the Au coated half needed a higher gate voltage (10-15V) than the uncoated half, i.e. the emission current scaled with the work function. This was not the case for the 4 Au coated samples as the initial gate voltage required to get the same anode current from each of them was similar to that from the uncoated array, which shows that the fraction of Au coated tips must be less.

The following is a method of estimating the fraction of the FEA area actually coated with Au (f). The assumptions are that the anode current from the Au coated

emitter tips, does not change due to the degradation. Also, the fraction of Mo remains the same throughout the experiment along with the tip geometry.

For the uncoated, 22Å Au coated and 44Å Au coated FEAs, we have different values of the initial gate voltage required to obtain 53mA, which are shown below :

V_g = 69.6 V (uncoated FEA)

V_g = 73.7 V (FEA coated with 22Å Au)

V_g = 70.5 V (FEA coated with 44Å Au)

Also, the value of degraded emission current for each of the above FEAs, after 100,000s (or 80,000L of O_2) is shown below:

I_a = 9.96mA (uncoated FEA)

I_a = 19.24mA (FEA coated with 22Å Au)

I_a = 13.32mA (FEA coated with 44Å Au)

For the 22 Å Au coated FEA,

V_g = 73.7 V

We can estimate the emission current from the uncoated area of the above FEA using the uncoated FEA I-V data. We substitute the value of Vg = 73.7 in the equation below :

$$\ln (I_a / V_g^2) = (-484.48 / V_g) \quad (5.8)$$

Solving the above equation yields, I_{Mo} = 88mA if the array were uncoated.

Now we have 2 equations to solve which are,

$$53 = 88 \times (1 - f) + I_{Au} \times (f) \quad (5.9)$$

$$19.24 = 9.96 \times (1 - f) + I_{Au} \times (f) \quad (5.10)$$

where I_{Au} is the emission current from the Au coated Tips.

Solving the above equations, we get f = **0.57** or **57**% Au coated tips.

For the 44 Å Au coated FEA,

$V_g = 70.5$ V

We can estimate the emission current from the uncoated area of the above FEA using the uncoated FEA I-V data. We substitute the value of Vg = 70.5 in the equation below :

$$\ln (I_a / V_g^2) = (-484.48 / V_g) \quad (5.11)$$

Solving the above equation yields, I_{Mo} = 60mA from the uncoated area of the FEA.

Now we have 2 equations to solve which are,

$$53 = 60 \times (1 - f) + I_{Au} \times (f) \quad (5.12)$$

$$13.32 = 9.96 \times (1 - f) + I_{Au} \times (f) \quad (5.13)$$

where I_{Au} is the emission current from the Au coated Tips.

Solving the above equations, we get f = **0.21** or **21**% Au coated tips.

The above results indicate that the emission current from the FEA having a higher fraction of Au coated tips (22Å Au) degraded to a lesser extent than that with a lower fraction (44Å Au). One reason for this discrepancy is that the thickness of the Au coating on the FEA may have been much less than 44Å, as it was not experimentally determined using RBS.

REFERENCES

[1] V.G. Litovchenko, A.A. Evtukh, R.I. Marchenko, N.I. Klyui, and V.A. Semenovich, Appl. Surf. Sci. **111**, 213, (1997).

[2] O. Auciello, J.C. Tucek, A.R. Krauss, D.M. Gruen, N. Moldovan, and D.C. Mancini, J. Vac. Sci. Technol. **B19**, 877, (2001).

[3] B.R. Chalamala, Y. Wei, G. Rossi, B.G. Smith, and R.H. Reuss, Appl. Phys. Lett. **77**, 3284, (2000).

[4] H. Busta, G. Gammie and S. Skala, "Pressure Dependency of Emission Currents of Si, Mo, Au, and SiC Field Emitters", Technical Digest of IVMC'96, St. Petersburg, USA, 1996, p. 143.

[5] M.S. Mousa, Vacuum. **45**, 241, (1993).

[6] J.H. Jung, B.K. Ju, Y.H. Lee, J. Jang, and M.H. Oh, J. Vac. Sci. Technol. **B17**, 486 (1999).

[7] W.B. Choi, J. Liu, M.T. McClure, A.F. Myers, V.V. Zhirnov, J.J. Cuomo, and J.J. Hren, J. Vac. Sci. Technol. **B14**, 2050 (1996).

[8] J.M. Macaulay, I. Brodie, C.A. Spindt, and C.E. Holland, Appl. Phys. Lett. **61**, 997, (1992).

[9] A.A. Talin, T.E. Felter, and D.J. Devine, J. Vac. Sci. Technol. **B13**, 448, (1995).

[10] P.R. Schwoebel, C.A. Spindt, and I. Brodie, J. Vac. Sci. Technol. **B13**, 338, (1995).

[11] M. Endo, H. Nakane, and H. Adachi, J. Vac. Sci. Technol. **B14**, 2114, (1996).

[12] W.A. Mackie, T. Xie, M.R. Matthews, B.P. Routh, Jr., and P.R. Davis, J. Vac. Sci. Technol. **B16**, 2057, (1998).

CHAPTER 6

SUMMARY AND CONCLUSIONS ALONG WITH FUTURE EXPERIMENTS

6.1. Summary and Conclusions

The interaction of active Mo field emitter arrays with O_2 was studied. Experiments were set up to measure the emission characteristics as a function of gas exposures, duty cycle and initial gate voltage. The changes in slope and y - intercept of the FN plot were recorded. The data obtained from these measurements was used in estimating the mean lifetime of FEAs under these conditions.

It was also found out that the pulsed mode degradation effects were similar to those done in DC mode. We coated several FEAs with Au of which two FEAs were coated with Au on one half their area, allowing us to do an in-situ comparison of the Au coated half to the uncoated half. The only drawback was that Au had a much lower initial current due to its high work function as compared to Mo.

Au coating the FEA improved the stability to O_2 degradation by almost 3 times. The Au coated half degraded some, indicating that there may be some fraction of uncoated emitting tips. Further more, we were able to estimate the fraction of uncoated tips using the data from these experiments.

We also deposited Au films of different thickness varying from 22Å to 90Å and studied their interaction with O_2 at a 5% duty cycle for 200,000s. This was 100x acceleration in the nominal exposure dose. The results were not as expected as the Au coated FEAs also showed similar degradation effects as the uncoated FEAs.

A possible explanation is that the FEAs were not completely coated with Au, which was seen from their I-V emission characteristics (F-N plots). The Au coated FEAs needed the same voltage to get a given emission current as the uncoated FEAs. These results differed from the FEAs coated with Au on half their emission area, where there was an increase of 10-15V in gate voltage for the Au coated half.

The other information we obtained from the F-N plots after these O_2 degradation experiments was that apart from an increase in slope, there was also a significant increase in the y - intercept after an O_2 degradation experiment. This indicated that the increase in emission area after the O_2 degradation experiment was either due to blunting of the emitting tip or more tips emitting.

6.2. Future Experiments

6.2.1 O_2 Degradation in Pulsed Mode

We need to perform long-term experiments at different duty cycles. This would give us a better understanding of the degradation when the device is switched off.

6.2.2 In-situ analysis of the Work function of the emitting tips

The limitations of the present equipment, would not allow us to calculate the average work function of the emitting tips. We would require an energy analyzer[1] where we can calculate the work function of the emitting tip and from the slope of the F-N plot, deduce the tip geometry (field enhancement) factor before and after the O_2 degradation experiment.

REFERENCES

[1] E.D. Sosa, P. Abbot, D.E. Golden, App. Phys. Lett. **78**, 3899 (2001)

APPENDIX

EXPERIMENTAL MEASUREMENTS

1. GATE POWER SUPPLY

1.1 Voltage Calibration

One of the first measurements was to calibrate the HP6209B[1] gate power supply using the HP59501B[2] power supply programmer. The calibration was done after setting the zero mark. The input voltage for the HP59501B[2] was set using Labview 6.0i[3] and the output voltage from the HP6209B[1] was measured using a Keithley 2700 multimeter[4], which was calibrated by measuring the voltage from a 9V Battery. The graph shown below, gives us the required relation between the input and output voltage

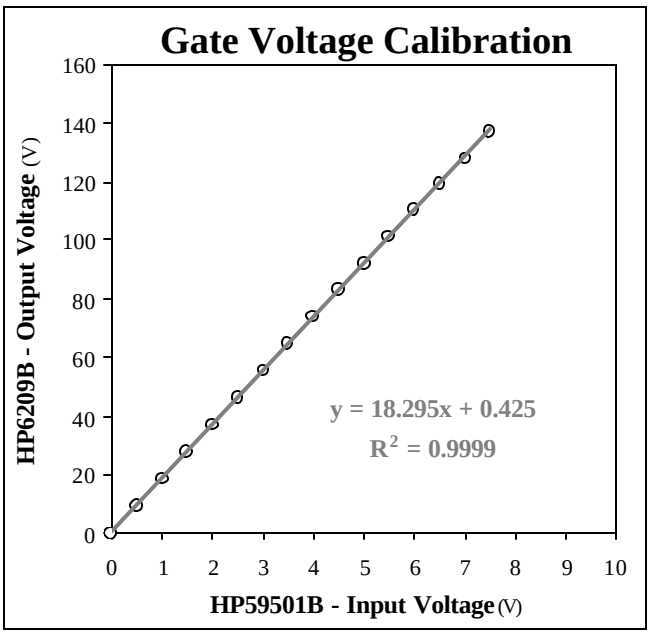

Figure 1. Graph showing voltage calibration for the gate power supply

The relation between the input voltage and the output gate voltage is as follows:

$$V_{out} = 18.295 \cdot V_{in} + 0.425 \quad (1)$$

The above equation can also be re-written to yield V_{in} as a function V_{out}, which is :

$$V_{in} = 0.0547 \cdot V_{out} - 0.0232 \quad (2)$$

2. LABVIEW CODES

2.1 Voltage Ramp

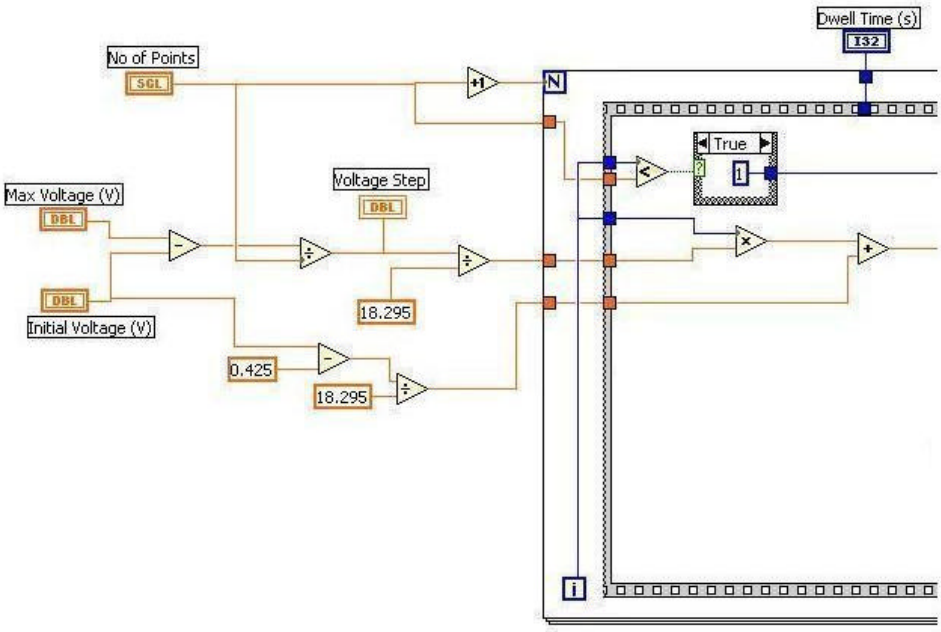

(a)

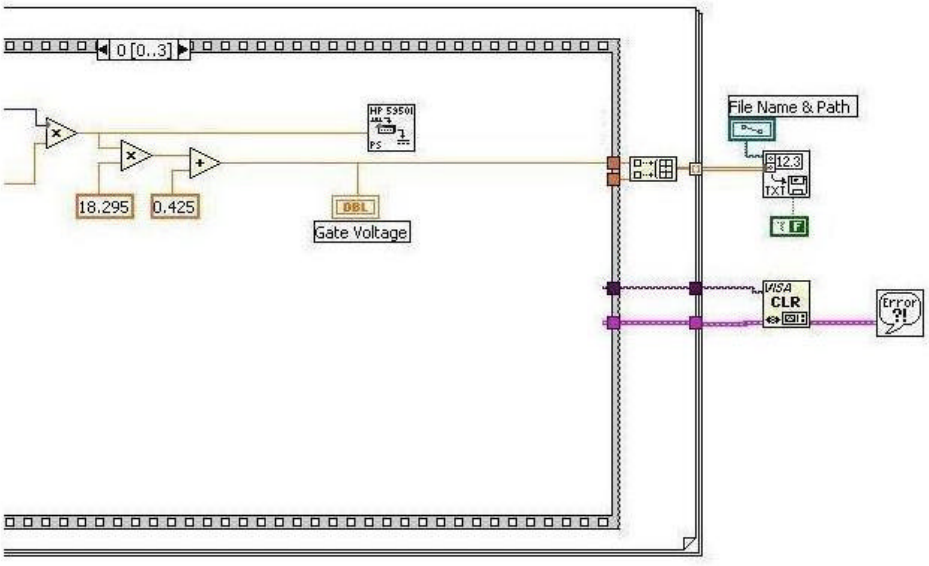

(b)

.

Figure 2 Voltage ramp block diagram. Fig 2 (a) shows the multiplying factors for converting the set power supply voltage into the programmer input voltage. The voltage ramp is done by the "For" loop. Fig 2 (b) indicates the programmer input voltage going into the HP59501B programmer.

2.2 DC Mode - Anode Current Measurement

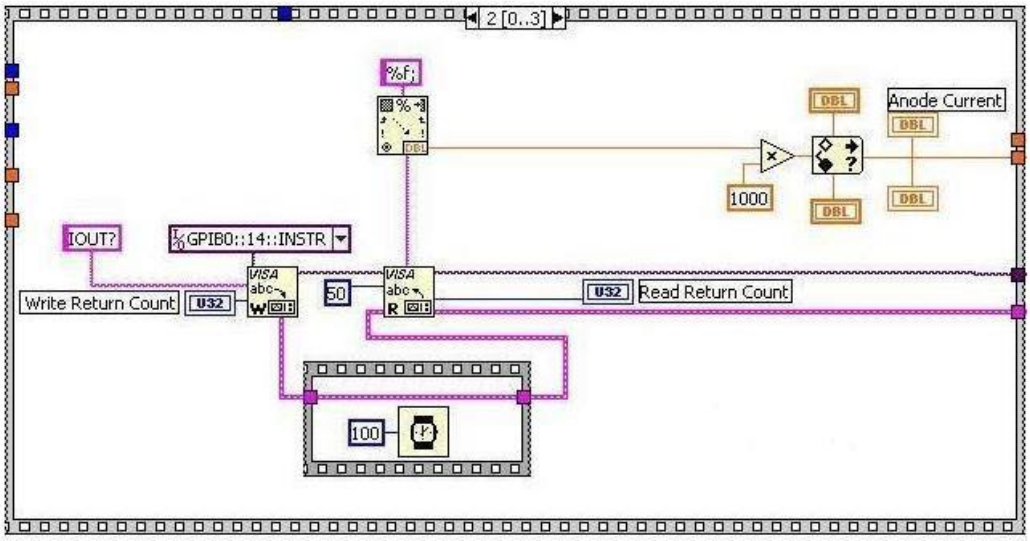

Figure 3 Measuring the anode current using the SRS350[5] power supply.

2.3 Exposure Dose

The dose was calculated by integrating (numerically) the area under the P-t curve.

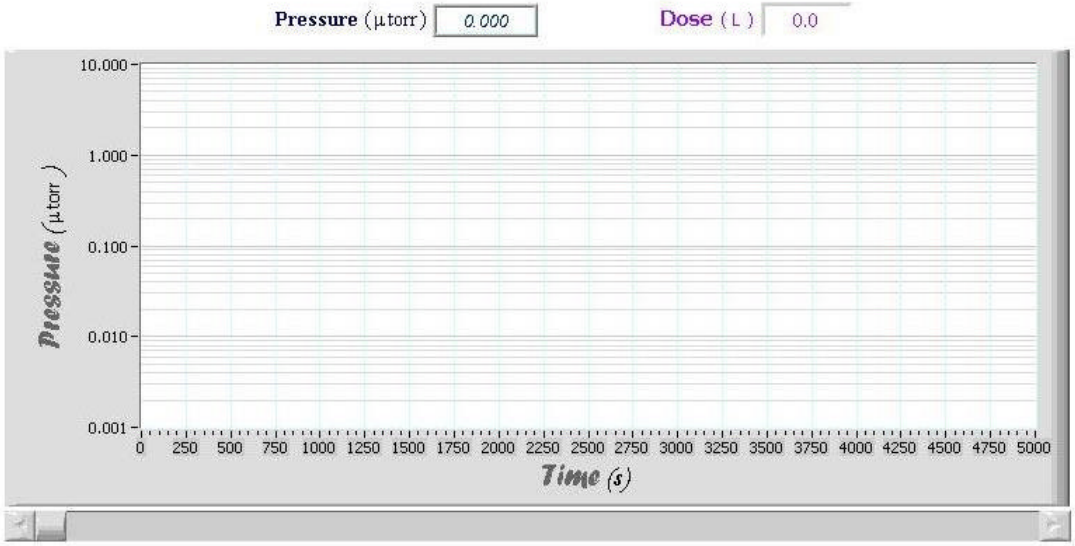

Figure 4 Front panel for the dose calculation from the pressure reading.

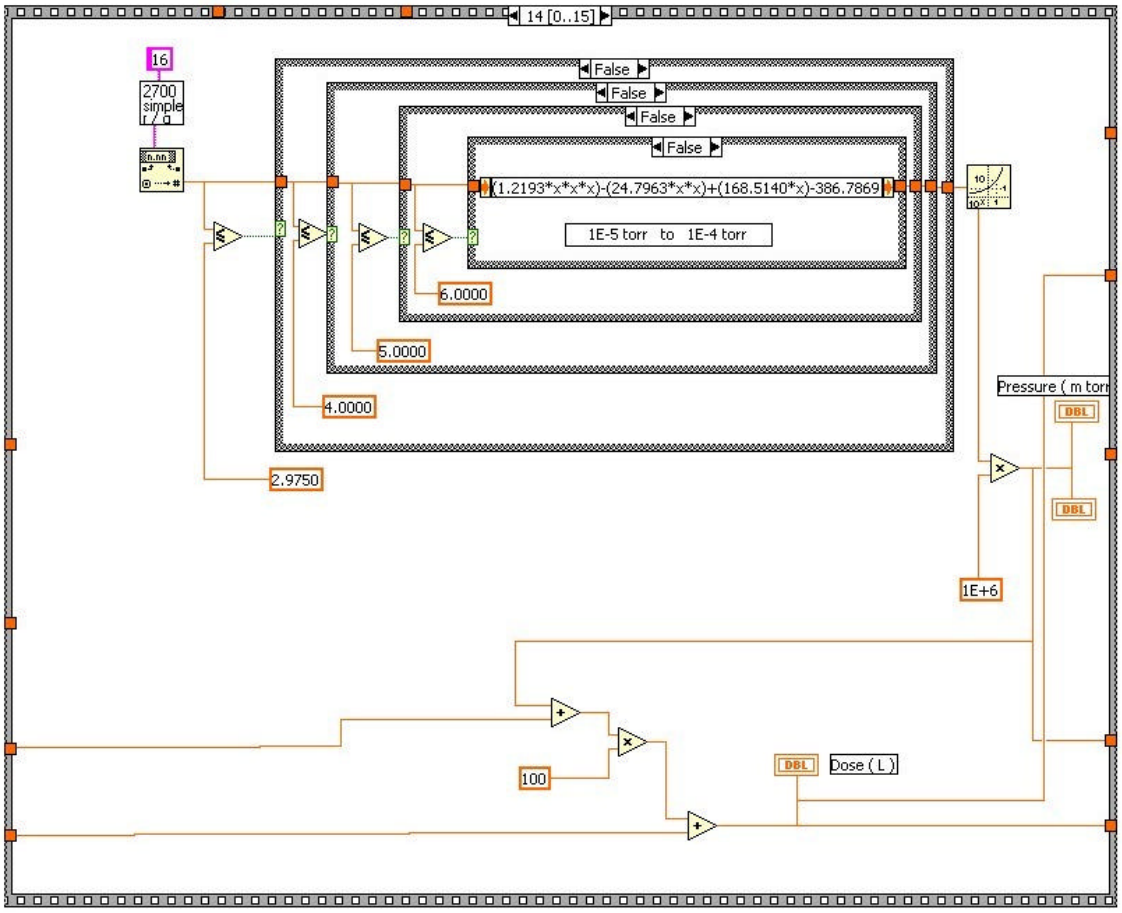

Figure 5 Block diagram showing the voltage read out from the Keithley 2700 multimeter[4] Depending on the range of the output voltage, the pressure is calculated using different case structures for different output voltages.

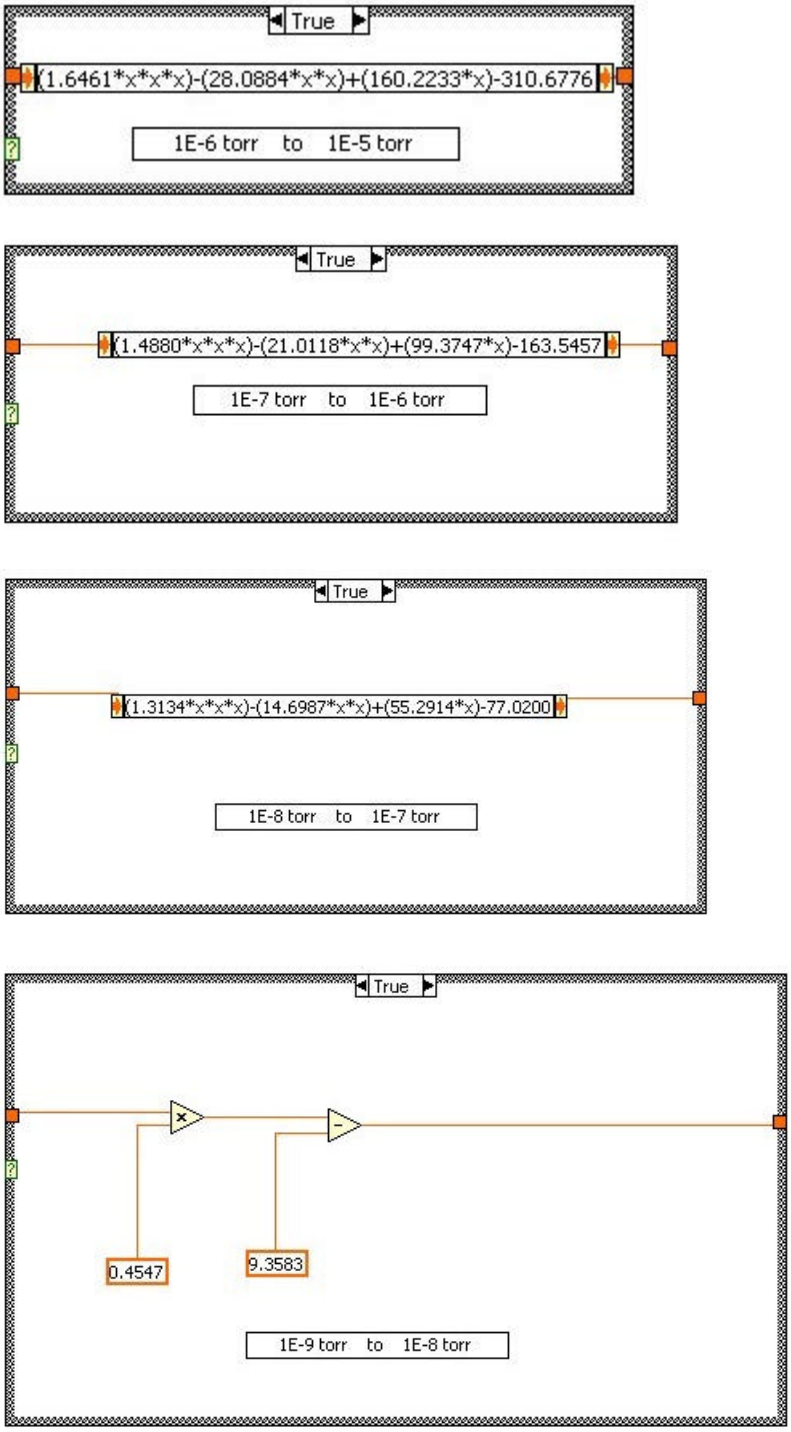

Figure 6 Different case structures for different pressure range conversions.

2.4 Setting the Duty Cycle

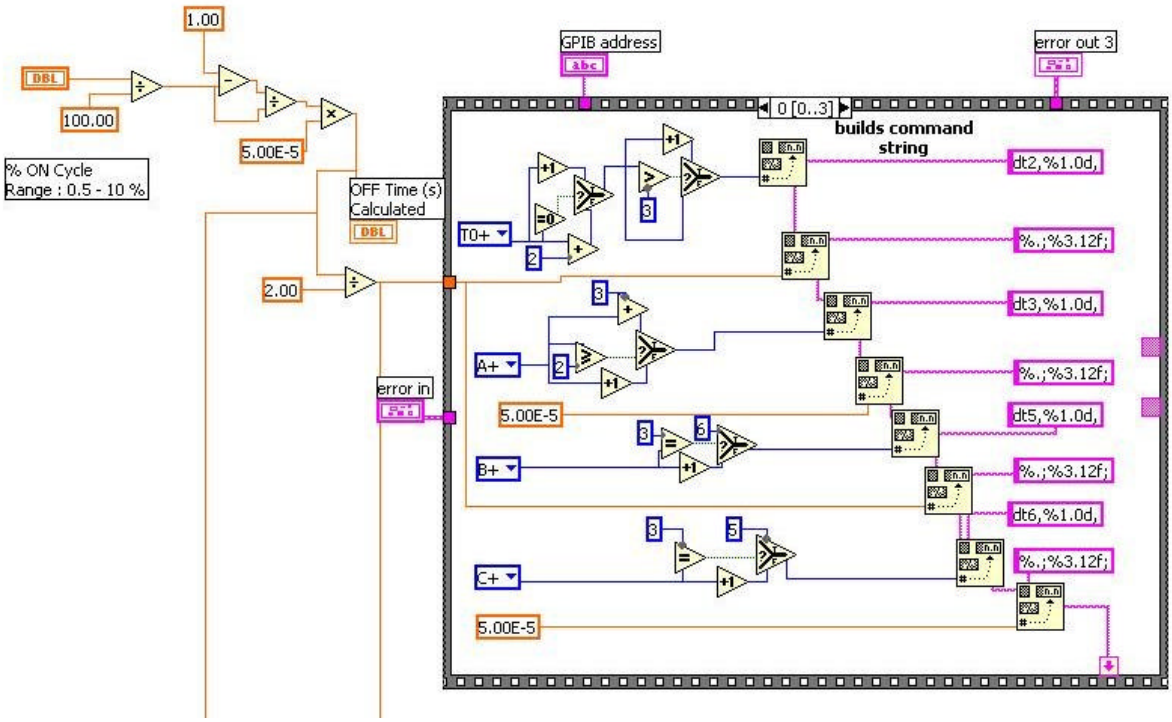

Figure 7 Block diagram for setting the "ON" duty cycle – Sequence 1

The above application uses an "ON" time of 50?s and calculates the "OFF" time using the following equation :

$$t_{Off} = t_{On} \times ((100 - R)/R) \quad (3)$$

where,

t_{On} = "ON" time (50?s)

R = % Duty Cycle

Once the OFF time is calculated, the values of t_{Off} and t_{On} are sent to the SRS VG535[5] dual channel function generator.

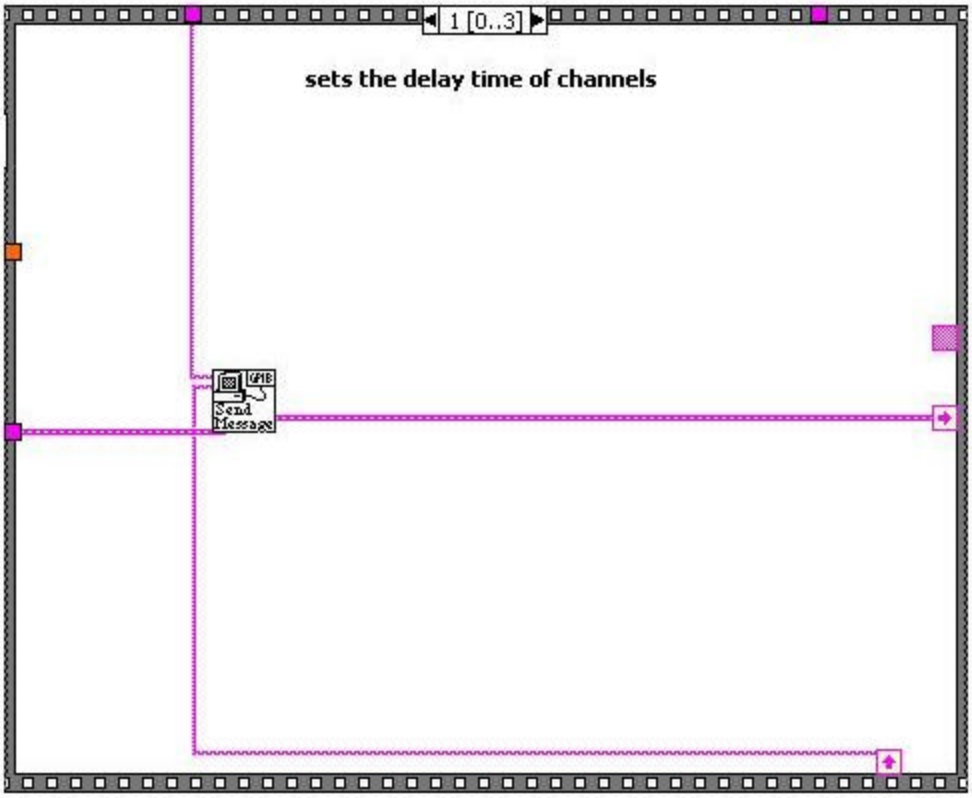

Figure 8 Block diagram for setting the “ON” duty cycle – Sequence 2

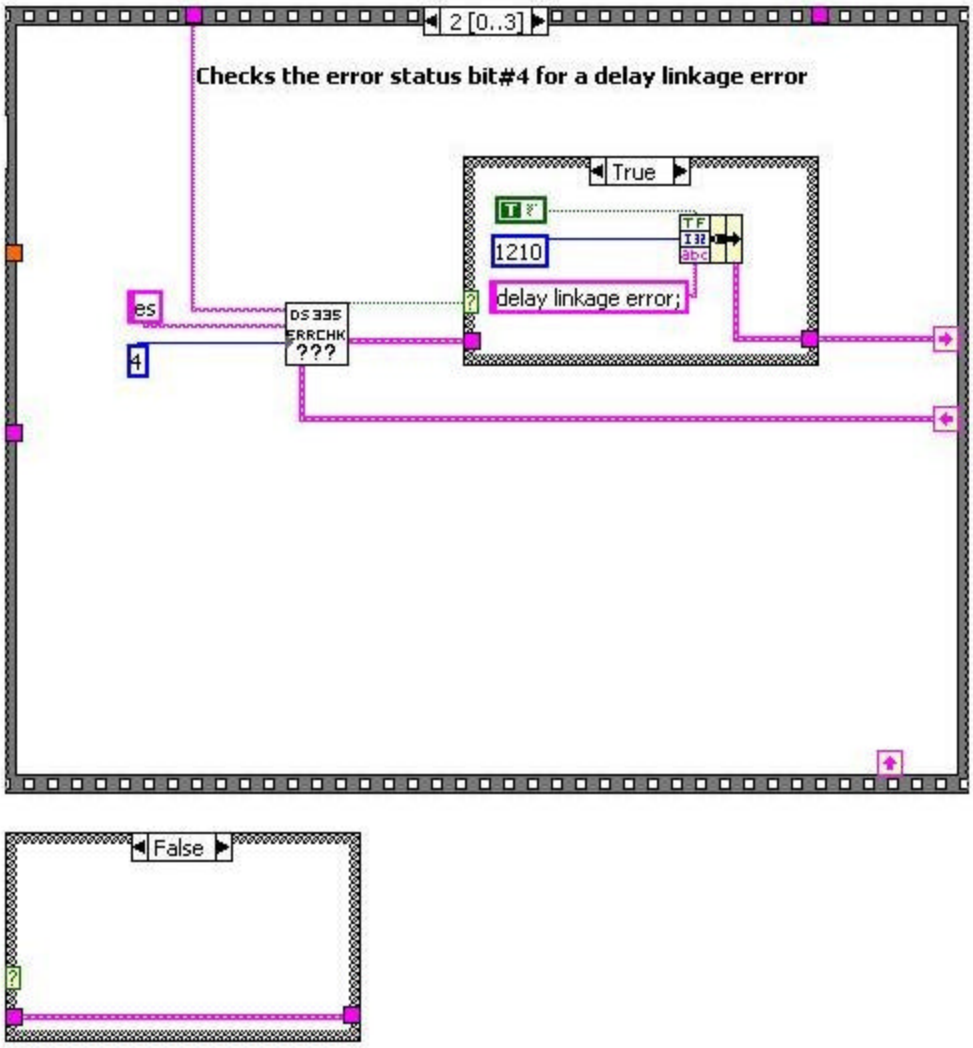

Figure 9 Block diagram for setting the “ON” duty cycle – Sequence 3

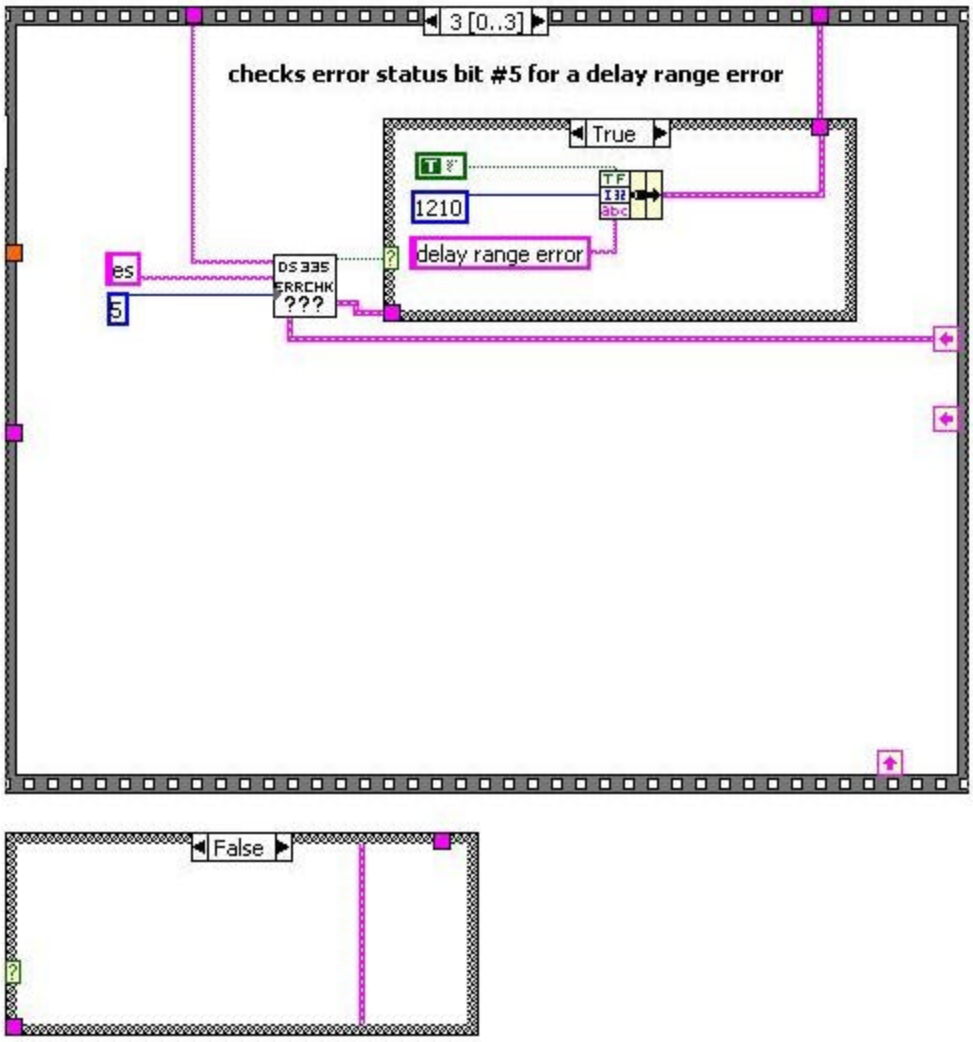

Figure 10 Block diagram for setting the “ON” duty cycle – Sequence 4

2.5 Pulsed Mode – Anode Current Measurement

The pulsed mode anode current measurements were made using a Lecroy 9310[6] digital oscilloscope. By measuring the voltage drop across the 330O resistor, we were able to calculate the anode current. Figures 11 – 15 show the various sequences for measuring the anode current for each of the 2 halves of the FEA.

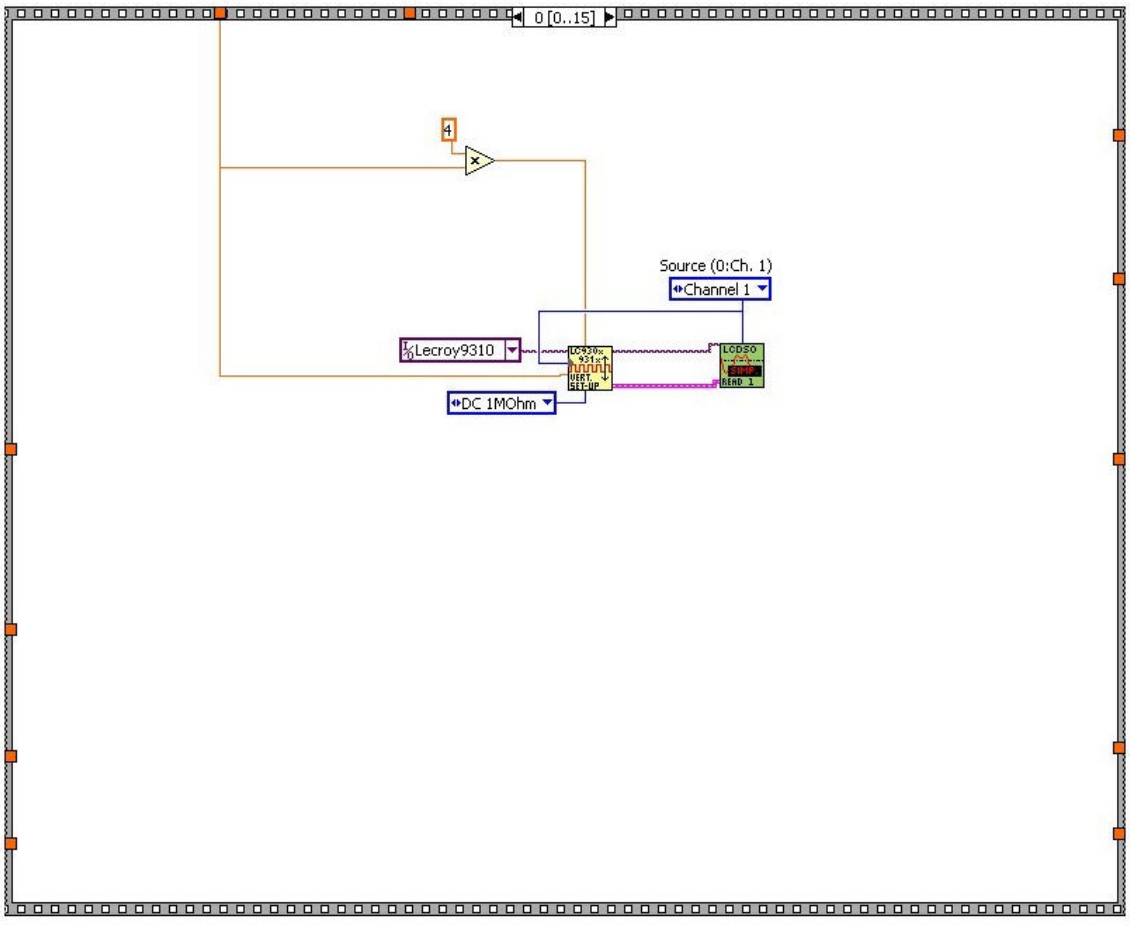

Figure 11 Block diagram 1 - Oscilloscope settings for channel 1 (trigger)

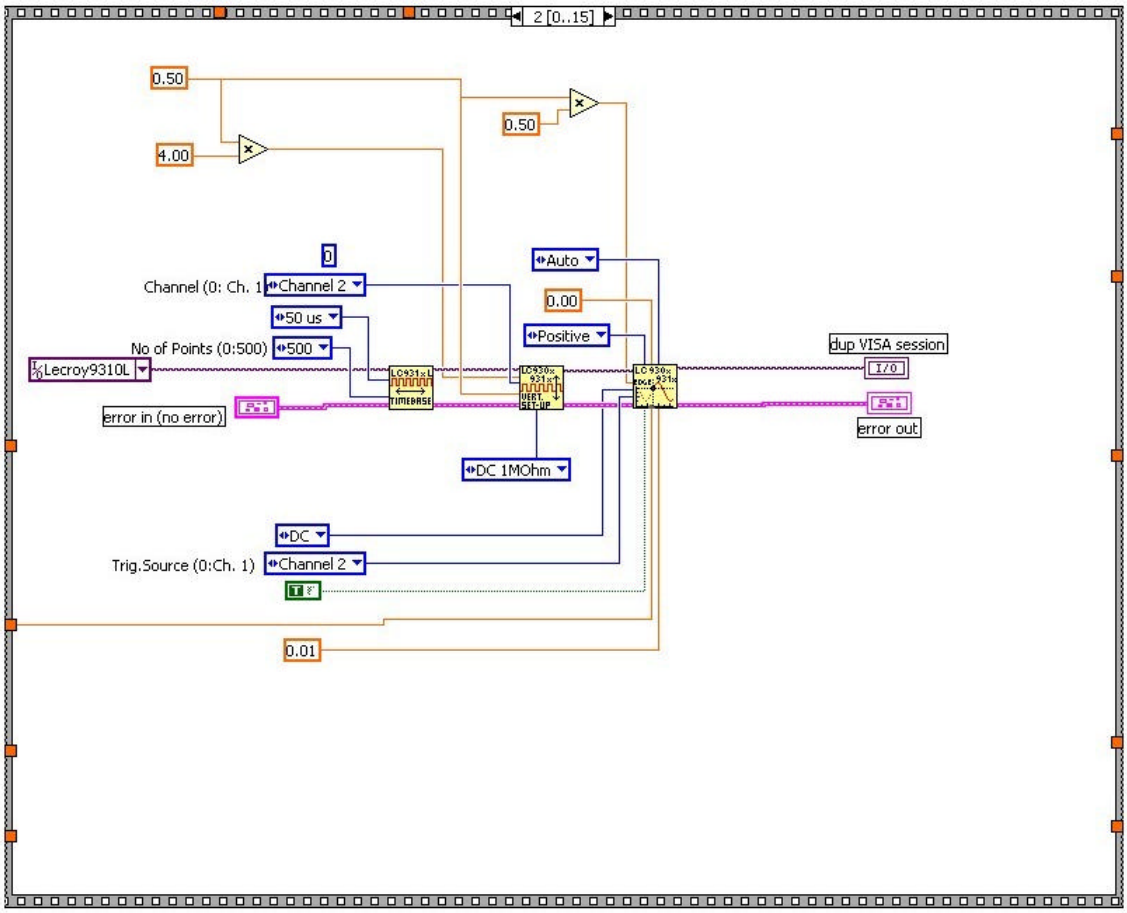

Figure 12 Block diagram 2 - Oscilloscope settings for the 1st half of the FEA (uncoated).

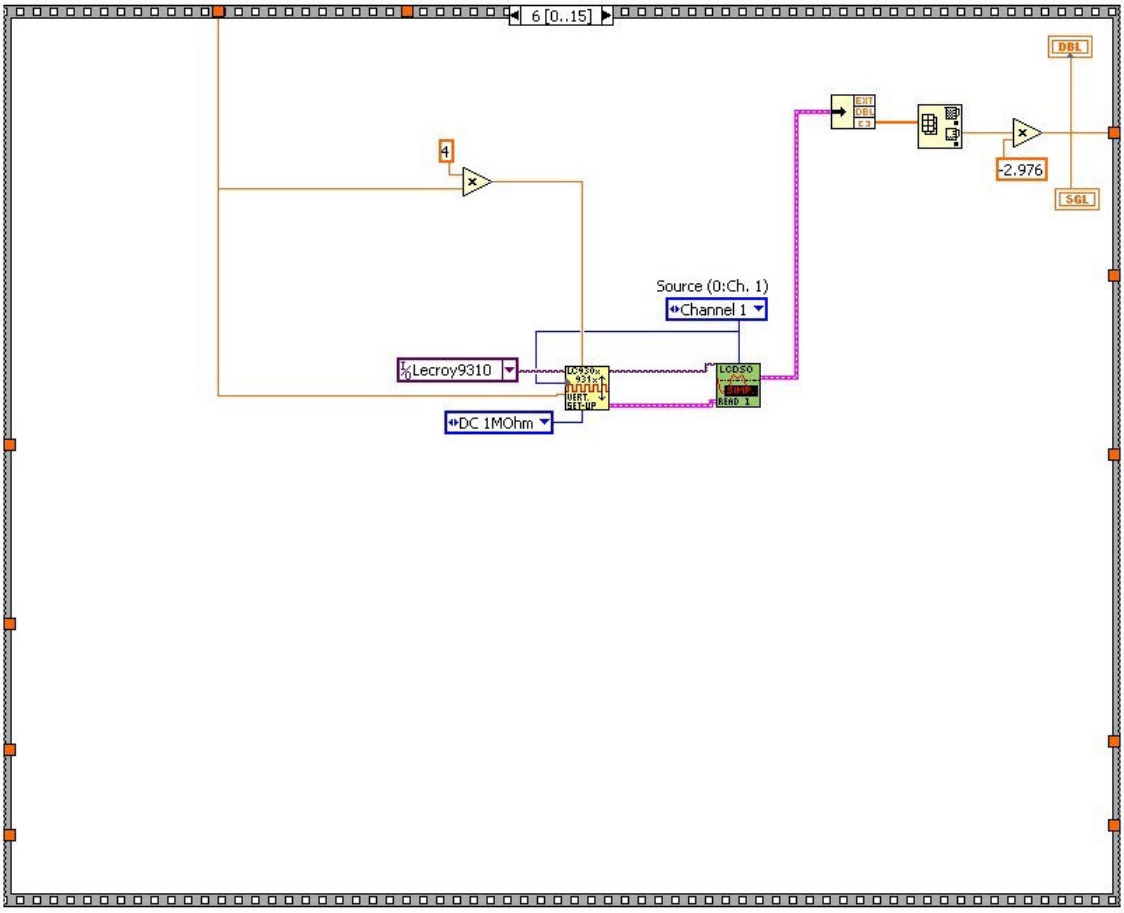

Figure 13 Block diagram 3 – Anode current from the 1st half of the FEA (uncoated).

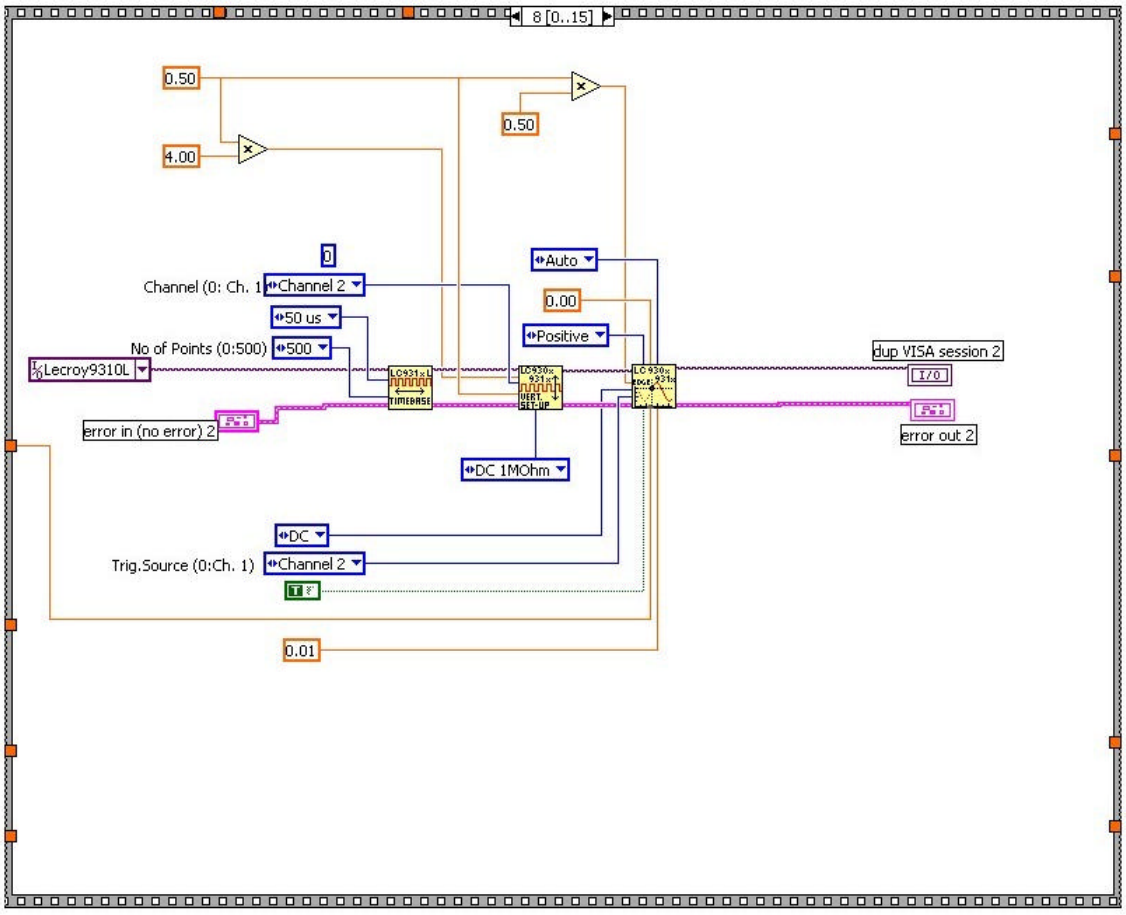

Figure 14 Block diagram 4 - Oscilloscope settings for the 2nd half of the FEA (Au coated).

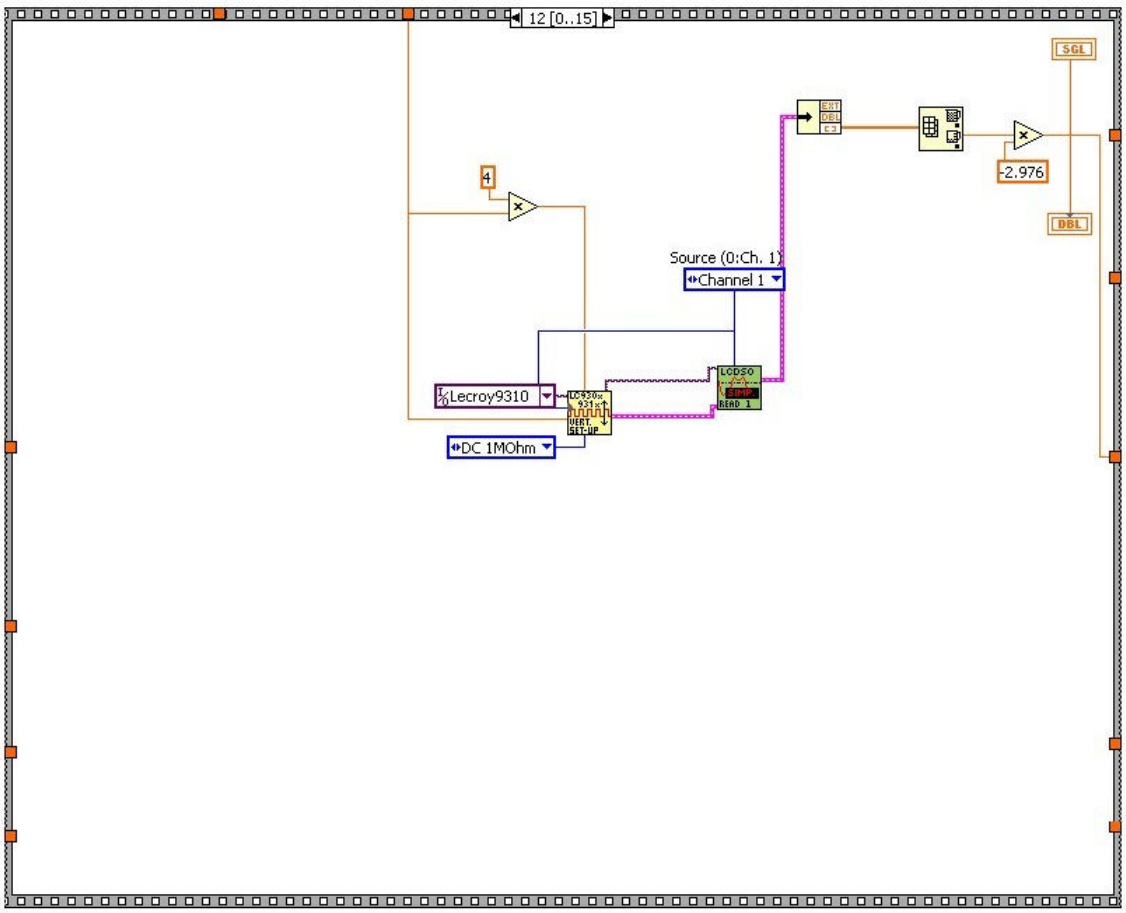

Figure 15 Block diagram 5 – Anode current from the 2nd half of the FEA (Au coated).

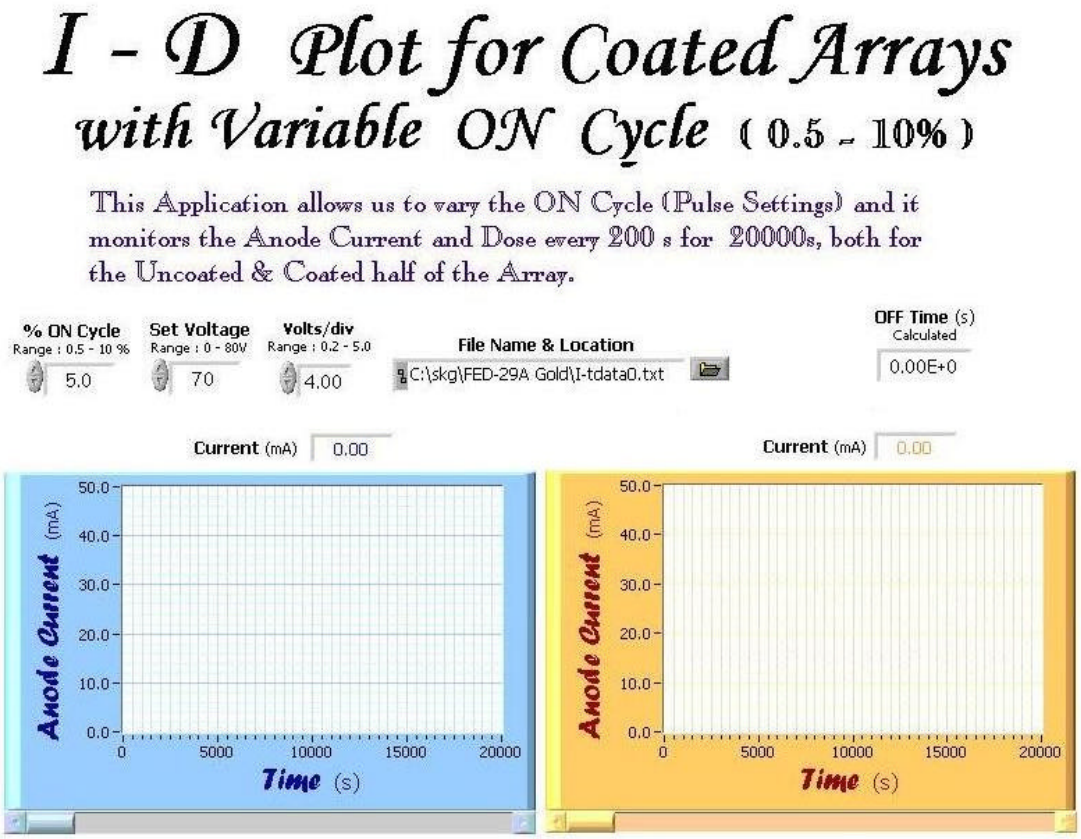

Figure 16 Front panel of the application for measuring the pulsed mode anode current from the uncoated half and the Au coated half of the FEA.

REFERENCES

[1] HP6209B DC Power Supply Manual.
[2] HP59501B Power Supply Programmer Manual.
[3] Labview^{TM} 6.0i is a registered trademark of National Instruments Inc., Austin, Texas (2000).
[4] Keithley 2700 Multimeter and Programmer Manual.
[5] Stanford Research Systems, Inc., 1290-D Reamwood Avenue, Sunnyvale, CA 94089.
[6] LeCroy 9310, 300 MHz dual channeled Oscilloscope Manual.